AD-A108 043 ANALYTIC SCIENCES CORP READING MA F/G 1/3
RESEARCH IN MULTIRATE ESTIMATION AND CONTROL--OPTIMAL SAMPLE RA--ETC(U)
OCT 81 D P GLASSON, J DOWD N00014-79-C-0431
UNCLASSIFIED TASC-TR-1356-2 NL

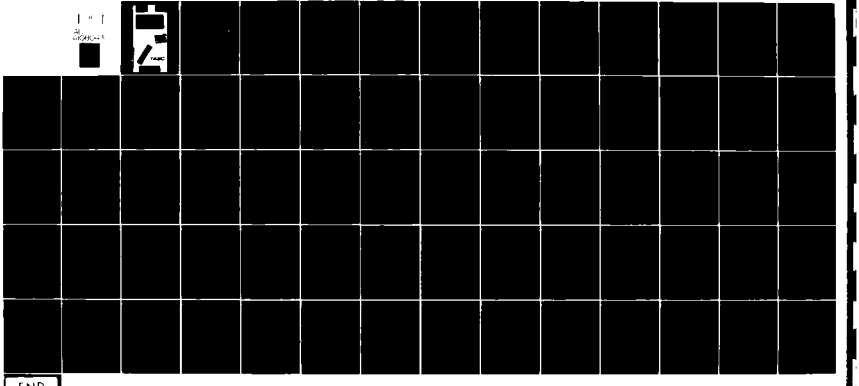

END
DATE FILMED
1 82
DTIC

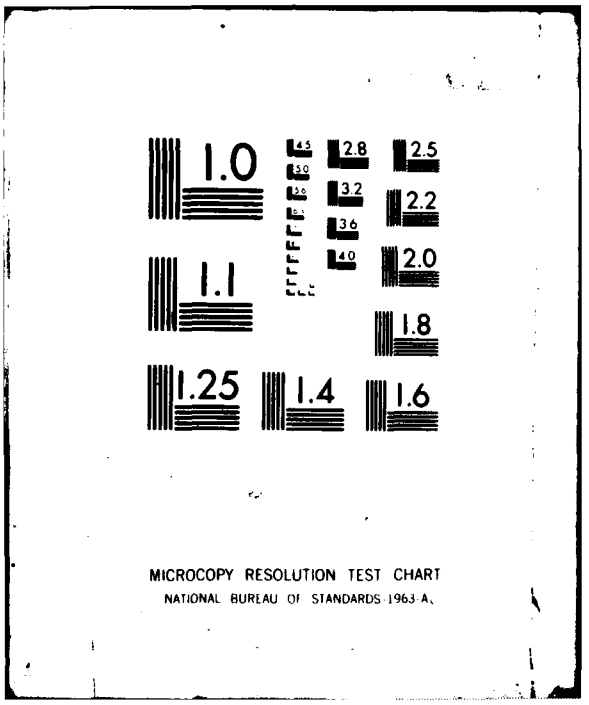
1.0
1.1
1.25
1.4
1.6
1.8
2.0
2.2
2.5
2.8
3.2
3.6
4.0
MICROCOPY RESOLUTION TEST CHART
NATIONAL BUREAU OF STANDARDS 1963-A

AD A108043

LEVEL II

12

DTIC
ELECTE
DEC 2 1981
H

DTIC FILE COPY

DISTRIBUTION STATEMENT A
Approved for public release;
Distribution Unlimited

TASC

ONE JACOB WAY READING, MASSACHUSETTS 01867 (617) 944-6850

81 12 02 036

THE ANALYTIC SCIENCES CORPORATION

(12)

TR-1356-2

RESEARCH IN MULTIRATE ESTIMATION AND CONTROL-OPTIMAL SAMPLE RATE SELECTION

8 October 1981

DTIC
ELECTE
DEC 2 1981
D

Prepared for:

Office of Naval Research
Arlington, VA.

Prepared by:

Douglas P. Glasson
Jeffery Dowd

Approved by:

James D. Shields
E. Wayne Vinje

THE ANALYTIC SCIENCES CORPORATION
One Jacob Way
Reading, Massachusetts 01867

DISTRIBUTION STATEMENT A
Approved for public release;
Distribution Unlimited

UNCLASSIFIED

SECURITY CLASSIFICATION OF THIS PAGE (When Data Entered)

REPORT DOCUMENTATION PAGE		READ INSTRUCTIONS BEFORE COMPLETING FORM
1. REPORT NUMBER TR-1356-2	2. GOVT ACCESSION NO. AD-A108 043	3. RECIPIENT'S CATALOG NUMBER
4. TITLE (and Subtitle) Research in Multirate Estimation and Control --Optimal Sample Rate Selection		5. TYPE OF REPORT & PERIOD COVERED 5/1/79 - 5/1/80 6. PERFORMING ORG. REPORT NUMBER TR-1356-2
7. AUTHOR(s) Douglas P. Glasson		8. CONTRACT OR GRANT NUMBER(s) N00014-79-C-0431
9. PERFORMING ORGANIZATION NAME AND ADDRESS The Analytic Sciences Corporation One Jacob Way Reading, Massachusetts 01867		10. PROGRAM ELEMENT, PROJECT, TASK AREA & WORK UNIT NUMBERS
11. CONTROLLING OFFICE NAME AND ADDRESS Office of Naval Research Arlington, Virginia		12. REPORT DATE October 1981 13. NUMBER OF PAGES 63
14. MONITORING AGENCY NAME & ADDRESS(if different from Controlling Office)		15. SECURITY CLASS. (of this report) Unclassified 15a. DECLASSIFICATION/DOWNGRADING SCHEDULE

16. DISTRIBUTION STATEMENT (of this Report)

Approved for public release; distribution unlimited.

17. DISTRIBUTION STATEMENT (of the abstract entered in Block 20, if different from Report)

18. SUPPLEMENTARY NOTES

19. KEY WORDS (Continue on reverse side if necessary and identify by block number)

Digital Control Systems
Flight Control Systems
Multiple Sample Rate Control
Optimal Control

20. ABSTRACT (Continue on reverse side if necessary and identify by block number)

A new algorithmic methodology for sample rate selection in multirate digital control design is developed. The methodology is based on optimizing the random disturbance rejection properties of a closed-loop multirate control structure under a computational constraint. The formulation and mathematical development of the multirate control design and sample rate selection procedure are presented; the sample rate selection

DD FORM 1 JAN 73 1473 EDITION OF 1 NOV 65 IS OBSOLETE

UNCLASSIFIED

SECURITY CLASSIFICATION OF THIS PAGE (When Data Entered)

20. ABSTRACT (Continued)

technique and properties of the resulting controllers are demonstrated through aircraft control examples.

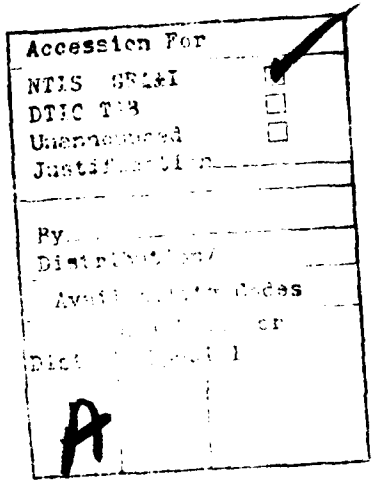

PREFACE

This investigation was conducted by The Analytic Sciences Corporation, Reading, Massachusetts, from 1 May 1980 through 20 April 1981, under Contract N00014-79-0431 for the Office of Naval Research, Arlington, VA. It was sponsored by the Mathematics Program headed by Dr. Stuart Brodsky. Dr. Charles Holland was the cognizant Navy Scientific Officer for final technical review and public release of this report.

Mr. Douglas P. Glasson was the principal investigator in this study. He was supported in this study by the technical contributions of Mr. Jeffery Dowd.

TABLE OF CONTENTS

LIST OF FIGURES

LIST OF TABLES

1. INTRODUCTION

1.1 BACKGROUND

The practical need for multiple sample rate control systems arises from the finite computational capabilities of digital computers used in control implementation. Although digital computer technology continues to advance significantly, particularly in the areas of distributed microprocessors and very large scale integration (VLSI), expanded computational capabilities are inevitably consumed in implementation. In aircraft applications, for example, new and expanded software requirements for such functions as control, navigation, display, and system monitoring tax the finite storage and computational capabilities of the flight computers. Accordingly, the flight control system designer is always allocated a fixed and usually limiting computational capability to implement a control design. In addition, accommodation of vehicle flexibility effects (in the form of instrument output filtering or active structural control) typically demands high sample rates -- rates that may be an order of magnitude higher than is necessary for suitable control of the rigid body modes of vehicle motion. Faced with widely varying sample rate requirements among the dynamic modes of the vehicle, a multirate control structure is the solution to onboard computational limitations.

In the first phase of the present research (reported in Ref. 1), a systematic methodology for designing multirate control systems was developed. This methodology, which is based on optimal estimation and control techniques, obviates dimensionality-growth problems inherent in classically-based techniques

(Refs. 2, 3, and 4) and provides a step-by-step procedure for converting a desired analog control design to an equivalent multirate design without approximation. In addition, the methodology is a design, as opposed to analysis, technique; the iterative trial-analysis-redesign process is avoided using the new technique.

The design technique developed in the first phase of this research required a priori specification of the sample rates for the system controls. In the present report, the issue of sample rate selection to optimize system performance under a computational constraint is addressed. A general mathematical formulation of this optimization problem and an algorithm structure to solve it are presented and illustrated through examples.

1.2 SUMMARY OF RESULTS

The major results obtained in this investigation are:

- Basic formulation of the optimal multirate estimator/regulator design problems
- Design-to-specification procedure for multirate control systems
- Extension of the multirate control design formulation to proportional-plus-integral control structures
- A covariance analysis methodology for periodic control structures
- Basic formulation of the optimal sample rate selection problem
- A general algorithm structure to solve the optimal sample rate selection problem
- Investigation of optimal sample rate solutions and closed-loop system properties through examples

The first four items listed were developed in the first phase of the research and are presented in detail in Ref. 1; hence, these items are only summarized in the present report. The remaining three accomplishments are the primary topics of the present report.

The basic formulation of the optimal sample rate selection problem involves the development of system performance metrics and computational requirement models as well as the combining of these two elements into a Hamiltonian function. Sufficient conditions for a stationary point of the Hamiltonian are then developed with due regard to the fact that integer-valued independent variables (related to the sample rates of slow controls) are involved in the formulation.

A gradient-like minimum-seeking algorithm is developed to solve the optimization problem. This algorithm is gradient-like in that a step-by-step search of the payoff set is performed by moving in steps of the independent variables that improve performance; the step sizes, however, are strictly prescribed owing to the fact that certain of the independent variables are integer-valued.

Two example applications of the sample rate selection technique are presented. The first example is the lateral dynamics of the space shuttle orbiter; in this example, the basic properties of the optimal sample rate selection methodology are demonstrated and effects of restricted computational budget on the optimal solution and resulting closed-loop system properties are evaluated. The second example is optimization of the longitudinal ride-qualities of the F-14 aircraft under a computational constraint. In the F-14 example, realistic models of atmospheric turbulence, which constitutes the disturbance to the system, are used and physically-motivated guidelines for

selecting the appropriate performance metric are prescribed. Also, variations of the optimal solution with flight condition are investigated and recommendations are made for practical control implementation based on the observed variations.

1.3 ORGANIZATION OF THE REPORT

Sample rate selection to optimize the performance of a multiple sample rate control system under a computational constraint is addressed in this report. An overview of the deterministic design procedure (developed in the first phase of the present research) is presented in Chapter 2 in addition to the problem statement, formulation, and solution methodology of the optimal sample rate selection problem. A prototype problem, based on a lateral control design for the space shuttle is also presented in Chapter 2. Application of the new sample rate selection technique to a practical aircraft design problem is presented in Chapter 3. Conclusions and recommendations for future research are presented in Chapter 4.

2. OPTIMAL SAMPLE RATE SELECTION

The purpose of this chapter is to outline the mathematical formulation and solution of the optimal sample rate selection problem and to illustrate the use of this technique in a prototype problem. The deterministic part of control system design (i.e., the design-to-specification procedure to obtain desired transient response characteristics from the multirate control system) was addressed in detail in Ref. 1; hence, the deterministic design procedure will only be summarized here. The problem statement for the present research is presented in Section 2.2; the corresponding mathematical formulation, derivation of optimality conditions, and solution methodology is covered in Section 2.3. An algorithm to solve the sample rate selection problem is described in Section 2.4. A prototype problem, based on disturbance rejection optimization of the space shuttle lateral controller, is solved and evaluated in Section 2.5. The chapter is summarized in Section 2.6.

2.1 SUMMARY OF THE DETERMINISTIC DESIGN TECHNIQUE

It is assumed that the plant dynamics to be controlled are described by the linear-time-invariant differential equation:

$$\dot{\underline{x}}(t) = F\underline{x}(t) + G\underline{u}(t) \qquad (2.1\text{-}1)$$

where $\underline{x}$ is the state vector and $\underline{u}$ is the control vector. The control $\underline{u}$ is to be sampled and held at time instants t_k, with all elements of $\underline{u}$ possibly sampled at different rates.

The discrete-time dynamics of the continuous plant are described by:

$$\underline{x}_{k+1} = \Phi \underline{x}_k + \Gamma_f \underline{u}_{f_k} + \Gamma_s \underline{u}_{s_k} \qquad (2.1\text{-}2)$$

where

$$\Phi = e^{FT_s}$$

$$\Gamma = \int_0^{T_s} e^{F\tau} G \, d\tau$$

and the control vector, $\underline{u}$, has been partitioned into subsets $\underline{u}_f$ and $\underline{u}_s$ to signify those controls computed at the base rate and those scheduled at lower rates, respectively.

Development of the multirate regulator structure requires augmentation of the natural plant dynamics by holding circuit states (i.e., to hold the slow controls between updates); the discrete-time dynamics of this augmented system (for the case of two sample rates) are given by:

$$\left[\begin{array}{c} \underline{x}_{k+1} \\ \hline \underline{u}_{s_{k+1}} \end{array}\right] = \left[\begin{array}{c|c} \Phi & \Gamma_s \\ \hline 0 & I \end{array}\right] \left[\begin{array}{c} \underline{x}_k \\ \hline \underline{u}_{s_k} \end{array}\right] + \left[\begin{array}{c|c} \Gamma_f & \Gamma_s \delta_{k,i\ell} \\ \hline 0 & I \; \delta_{k,i\ell} \end{array}\right] \left[\begin{array}{c} \underline{u}_{f_k} \\ \hline \underline{v}_k \end{array}\right] \qquad (2.1\text{-}3)$$

where $\delta_{k,i\ell}$ is the Kronecker delta function.

The structure of a multirate optimal regulator for the case of two sample rates is shown in Fig. 2.1-1. As the block diagram indicates, one control channel, $\underline{u}_f$, is updated at a fast rate, T_s^{-1} samples per second; $\underline{u}_s$ is computed at a slower rate, $(\ell T_s)^{-1}$ samples per second, and is held between

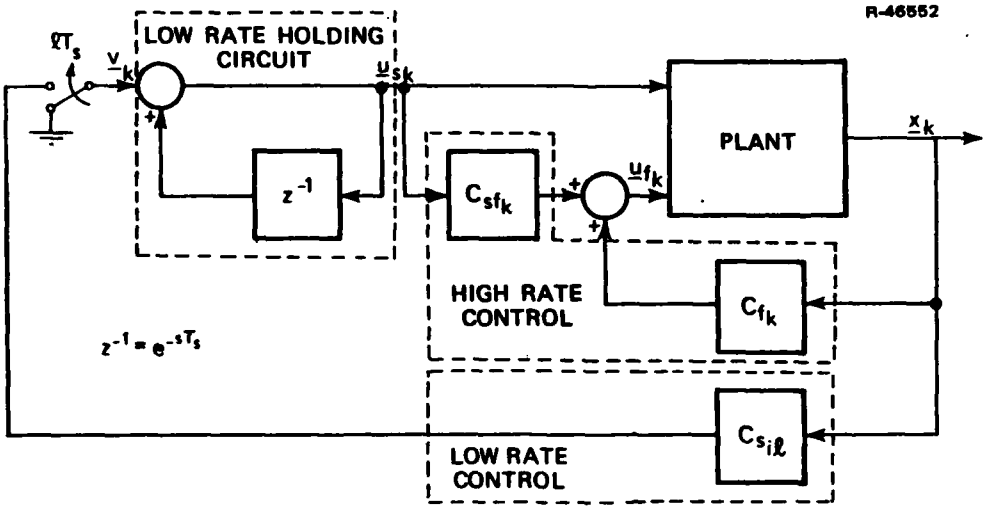

Figure 2.1-1 Multirate Regulator Structure

computations by a holding circuit. Recomputation of $\underline{u}_s$ is accomplished by adding an increment, $\underline{v}_k$, to the holding circuit on cycles when $k = i\ell$; on all other cycles $\underline{v}_k$ is set to zero. Another result of the present design procedure is that the slow control is crossfed to the fast control channel. The purpose of the crossfeed is to compensate excitations of the fast modes of the plant caused by $\underline{u}_s$ on cycles between slow control updates.

The periodic gains -- C_{f_k}, $C_{f_{i\ell}}$ and C_{sf_k} -- are obtained by propagating the optimal regulator Riccatti equation from infinity backwards to (periodic) steady state. The derived periodic regulator gains are:

$$C_k = \left[\begin{array}{c|c} C_{f_{i\ell}} & C_{sf_{i\ell}} \\ \hline & C_{s_{i\ell}} \end{array}\right] \quad ; \quad k = i\ell \qquad (2.1\text{-}4)$$

$$C_k = \left[C_{f_k} \;\vdots\; C_{sf_k}\right] \quad ; \quad k \neq i\ell \qquad (2.1\text{-}5)$$

Note that the dimensions of C_k change according to the number of controls that are computed on cycle k.

The closed-loop dynamics of the multirate system are determined by the choice of the quadratic cost functional weighting matrices used in the optimal regulator problem; i.e., with the following definition of the cost functional:

$$J = \frac{1}{2} \sum_{k=0}^{\infty} \{(\underline{x}_k^T \; \underline{u}_{s_k}^T) \; \hat{Q}_k \begin{pmatrix} \underline{x}_k \\ --- \\ \underline{u}_{s_k} \end{pmatrix} + 2(\underline{x}_k^T \; \underline{u}_{s_k}^T) \; \hat{M}_k \; \tilde{\underline{u}}_k$$

$$+ \tilde{\underline{u}}_k^T \; \hat{R}_k \; \tilde{\underline{u}}_k\} \qquad (2.1\text{-}6)$$

The choice of the matrices, $\hat{Q}_k$, $\hat{M}_k$, and $\hat{R}_k$, ultimately determines the dynamics of the closed-loop system. A procedure is described in Ref. 1 for deriving the $\hat{Q}_k$, $\hat{M}_k$, and $\hat{R}_k$, matrices from the weighting matrices of a specified continuous-time regulator design (for the continuous plant dynamics given by Eq. 2.1-1). This procedure is summarized here:

(1) A continuous-time regulator is designed to meet continuous-time performance specifications.

(2) Discrete-time regulator weighting matrices for the single rate case are derived from those used to design the continuous-time regulator.

(3) The discrete-time periodic weighting matrices used to solve for the multirate gains are constructed from the single rate matrices. The multirate gains are derived from the periodic steady-state solution of the discrete-time Ricatti equation.

The first step involves the normal iterative design process associated with designing an optimal regulator; i.e., trial

and error assignment of weighting matrix elements to yield a regulator that meets the design specifications. The relationships presented in Ref. 10 are then used to compute the single-rate (i.e., fast rate) discrete-time weighting matrices from the continuous-time matrices. Using the augmented system representation, Eq. 2.1-3 and the relationships in Ref. 10, expressions are derived for the multirate weighting matrices; inspection of these expressions indicates that the multirate matrices can be constructed from the single-rate matrices computed in step (2) above. An implicit benefit of this three-step approach is that the deterministic performance of the continuous-time, single-rate discrete-time, and multirate discrete-time controllers can be compared on a one-to-one basis; i.e., each control design is based on optimizing the same continuous-time cost functional (Ref. 10).

Extension of the two-sample-rate control structure described here to the multirate case (i.e., more than two sample rates) is straight-forward. Consider organizing the plant inputs into two groups: those computed at the fastest rate, $\underline{u}_f$, and those scheduled at lower rates, $\underline{u}_s$. Again augmenting the plant dynamics with slow control holding circuits (which now are operating at multiple rates) the discrete time dynamics of the augmented system are given by:

$$\begin{bmatrix} \underline{x}_{k+1} \\ \hline \underline{u}_{s_{k+1}} \end{bmatrix} = \left[\begin{array}{c|c} \Phi & \Gamma_s \\ \hline 0 & I \end{array}\right] \begin{bmatrix} \underline{x}_k \\ \hline \underline{u}_{s_k} \end{bmatrix} + \left[\begin{array}{c|c} \Gamma_f & \Gamma_s \Delta_k \\ \hline 0 & I\ \Delta_k \end{array}\right] \begin{bmatrix} \underline{u}_{f_k} \\ \hline \underline{v}_k \end{bmatrix} \qquad (2.1\text{-}6)$$

where

$$\Delta_k = \begin{bmatrix} \delta_{k,i_1\ell_1} & 0 & \cdots & 0 \\ 0 & \delta_{k,i_2\ell_2} & & \vdots \\ \vdots & & 0 & \vdots \\ 0 & \cdots & 0 & \delta_{k,i_{m'}\ell_{m'}} \end{bmatrix} \qquad (2.1\text{-}7)$$

where m' is the dimension of $\underline{v}$ and

$$\delta_{k,i_j\ell_j} = \begin{cases} 1; & i_j\ell_j = k \\ 0; & i_j\ell_j \neq k \end{cases} \qquad (2.1\text{-}8)$$

The matrix Δ_k is a generalization of the Kronecker delta functions used in the two-sample-rate case. Each diagonal element of Δ_k nulls the input to a particular low rate control holding circuit on cycles between new computations of that control. For example, if u_{s2} is computed every two cycles (i.e., $\ell_2 = 2$) then the second diagonal element of Δ_k will be zero on cycles when k is not a multiple of two (i.e., $k \neq i_2\ell_2$).

Again, the deterministic design procedure outlined in this section maintains consistency of transient response characteristics in proceeding from a desirable continuous-time design to a multirate digital implementation. In the following sections, the issue of optimizing stochastic error rejection properties under computational constraint is addressed. Uniformity of the deterministic properties of the control system, as the control sampling policy is varied, is implicit in the discussion that follows as a result of using the design procedure described here.

2.2 PROBLEM STATEMENT

The issue addressed in the present research is the selection of sample rates for a multirate digital control structure to optimize rejection of a stochastic disturbance while accommodating a computational constraint. An important digital control application that fits the general problem framework described here is optimization of digitally-controlled aircraft ride qualities (performance) while flying in a turbulent atmosphere (disturbance) under computational rate limitations of the onboard computer (constraint). In subsequent sections of this report, the formulation and solution technique described here will be illustrated in typical aircraft applications.

The mathematical problem statement is presented in Table 2.2-1. The plant dynamics are described by a linear-time-invariant stochastic differential equation. The form of the plant dynamics shown in Table 2.2-1 includes the case of a correlated process (such as a Markov model of atmospheric turbulence) disturbing the physical plant to be controlled; in this case the state vector, $\underline{x}$, includes the states of the disturbance process and the dynamics matrix, F, includes blocks defining the disturbance dynamics and its couplings to the physical plant.

The deterministic control design is based on optimizing an infinite-time-horizon quadratic cost functional, J_c, (specified in its continuous-time form in Table 2.2-1) under the constraint of piecewise constant controls computed at multiple rates. In the subsequent formulation, the continuous-time form of the quadratic cost functional will be converted to its equivalent multirate discrete-time form by the three-step procedure described in Section 2.1; hence, uniformity of the deterministic properties of the control design, as the control computation schedule is varied, is implicit in the present formulation.

TABLE 2.2-1
PROBLEM STATEMENT

- Given:

  Continuous-Time Plant Dynamics (Linear-Time-Invariant Stochastic)

  $$\dot{\underline{x}} = F\underline{x} + G\underline{u} + \Lambda\underline{w} \quad ; \quad w_i \sim N(0,\sigma_i)$$

  Control Design Cost Functional (Deterministic Dynamics)

  $$J_c = \frac{1}{2}\int_0^\infty \{\underline{x}^T Q\underline{x} + \underline{u}^T R\underline{u}\}\, dt$$

  Error Rejection Functional:

  $$J = \frac{1}{2}\sum_{k=1}^{\ell} W_k P_k W_k^T$$

  Computational Constraint:

  $$f_c \frac{T_s}{nt_m} - \frac{1}{\ell}\sum_{i=1}^{m} N_i = 0$$

where

f_c = fraction of computation rate capability allocated to control

n = number of multiplications per control channel

t_m = execution time for multiplication

T_s = base sample period

N_i = number of times control i is computed per control period

- Goal of the Optimization:

  Determine the sample period, T_s, and sample policies, N_i, that minimize the error rejection cost functional under the computational constraint

The performance to be optimized is expressed by the error rejection functional, J. In the form shown in Table 2.2-1, the performance functional represents the mean-squared value (in steady state) of a linear combination of the plant and disturbance states; i.e.:

$$a_k = W_k \underline{x}_k \tag{2.2-1}$$

$$E[a^2] = E[\frac{1}{\ell} \sum_{k=1}^{\ell} (W_k \underline{x}_k)(W_k \underline{x}_k)^T] \tag{2.2-2}$$

$$= \frac{1}{\ell} \sum_{k=1}^{\ell} W_k P_k W_k^T \tag{2.2-3}$$

Since the state error covariance matrix, P_k, of the closed-loop multirate system is periodic with period ℓ, a_k will also be periodic; hence, a summation over ℓ cycles and normalization by the $1/\ell$ factor are included in Eq. 2.2-3. The elements of the weighting array, W_k, are chosen according to the judgement of the designer or they may be derived on a physical basis. In an aircraft application, for example, a_k may be a physical quantity, such as a component of vehicle acceleration; the elements of W_k can then be derived from the coefficients of the differential equation describing that acceleration.

The computational constraint is a simple expression of the fact that a finite amount of computing capability is available for implementation of the control. The first term of the constraint equation is the computation budget. The numerator of the first term, $f_c T_s$, is the portion of each base sample period allocated to control computations; the denominator, nt_m, is an approximation of the computational time required to compute one control channel (i.e., element of $\underline{u}$); hence, the first

term represents a specification of the maximum allowable number of control computations per base sample period (averaged over ℓ cycles). The second term of the constraint equation is the total number of control channel computations over the ℓ cycle control schedule (normalized to a single base sample period by the $1/\ell$ factor). The equality expressed by the constraint equation stipulates that the total computational requirement of the control implementation should equal the available computational resources.

The goal of the optimization problem is to determine the values of the independent variables, T_s and the N_i's, that minimize the error rejection cost functional, J, under the specified computational constraint. In the following section, the formulation and algorithmic solution of this optimization problem are described.

2.3 MATHEMATICAL FORMULATION OF THE OPTIMIZATION PROBLEM

The problem statement outlined in Section 2.2 can be cast into a formal mathematical framework by constructing a Hamiltonian function that couples the performance measure and the computational constraint. The form of the Hamiltonian chosen for the present work is given below:

$$H = J + \lambda C \tag{2.3-1}$$

$$= \frac{1}{\ell} \sum_{k=1}^{\ell} W_k P_k W_k^T + \lambda \left(f_c \frac{T_s}{n t_m} - \frac{1}{\ell} \sum_{i=1}^{m} N_i \right) \tag{2.3-2}$$

The Hamiltonian is constructed by adjoining the constraint to the performance function using a Lagrange multiplier, λ. Owing to the equality constraint that C=0 at the stationary point of H:

$$H^* = J^* \qquad (2.3\text{-}3)$$

where J^* is the minimum value of the error rejection functional with the computational constraint satisfied.

Finding sufficient conditions for a minimum of the Hamiltonian (and, hence, the error rejection functional) requires consideration of the fact that some of the independent variables of the problem are integer-valued (i.e., the N_i's). The optimization strategy in this case will be to use the usual zero partial derivative condition for the continuous variables (T_s and λ) and specify that the Hamiltonian should be nondecreasing with respect to permissible (integer) changes in the N_i's about the stationary point. Mathematically, the optimality conditions are:

$$1)\quad \frac{\partial H}{\partial T_s} = \frac{1}{\ell} \sum_{k=1}^{\ell} W_k \frac{\partial P_k}{\partial T_s} W_k^T + \lambda \left(f_c \frac{1}{n t_m} \right) = 0 \qquad (2.3\text{-}4)$$

$$2)\quad \frac{\partial H}{\partial \lambda} = f_c \frac{T_s}{n t_m} - \frac{1}{\ell} \sum_{i=1}^{m} N_i = 0 \qquad (2.3\text{-}5)$$

3) H Nondecreasing with respect to changes in N_i's

At this point, an optimization scheme based on enumeration and search is seen to be a possible approach; Eq. 2.3-5 could be used to compute all permissible combinations of the independent variables, then all combinations could be tested to determine the set that yields the best error rejection (i.e., minimum J). In the present work, optimality conditions 1 and 2 are combined to allow more flexibility in choosing trial sets of the independent variables and the search over the trial sets is done systematically. The development of this approach is outlined here.

Using optimality condition 1, given by Eq. 2.3-4, a useful interpretation of the Lagrange multiplier and Hamiltonian is obtained. Optimality condition 1 can be written as:

$$\frac{\partial H}{\partial T_s} = \frac{\partial J}{\partial T_s} + \lambda \frac{\partial C}{\partial T_s} = 0 \qquad (2.3\text{-}6)$$

$$\therefore \quad \lambda = - \frac{\partial J}{\partial C} \qquad (2.3\text{-}7)$$

Using Eq. 2.3-7, the Hamiltonian can be rewritten:

$$H = J - \frac{\partial J}{\partial C} C \qquad (2.3\text{-}8)$$

At points where C takes on nonzero values:

$$C = - \Delta C \qquad (2.3\text{-}9)$$

where ΔC is the change in the constraint, affected by changing T_s <u>alone</u>, required to satisfy optimality condition 2 (Eq. 2.3-5). Hence:

$$H = J + \frac{\partial J}{\partial C} \Delta C \qquad (2.3\text{-}10)$$

Equation 2.3-10 suggests that the Hamiltonian can be interpreted as a two-term Taylor series approximation of the error rejection functional with the N_i's fixed and T_s adjusted to satisfy the computational constraint. This Taylor series interpretation is very useful; it suggests that the search over the N_i's can be done at a fixed value of T_s using the Hamiltonian to project the performance function from the trial point (where the constraint may not be satisfied) to the appropriate value of T_s. An optimization algorithm that uses this interpretation of the Hamiltonian is described in the following section.

2.4 OPTIMIZATION ALGORITHM

An optimization algorithm to search over the integer-valued N_i's is shown in Fig. 2.4-1. The starting point is a single-rate controller at a suitable value of T_s (i.e., all N_i's equal to ℓ and T_{so} chosen with due regard to the sampling theorem). The performance (Hamiltonian) of this single rate system is used to initialize the search over the N_i's. As shown in Fig. 2.4-1, the search algorithm has an outer-loop which compares the values of the Hamiltonian obtained from various combinations of the N_i's (looking for a minimum) and an inner-loop that generates the combinations of the N_i's.

The inner-loop operates by sorting through the controls one at a time, decrementing N_i for each control to its next lower integer value, and computing the Hamiltonian. If the Hamiltonian for the decremented N_i is lower than that for the previous value of N_i, N_i is set to the decremented value; if not, it is assumed that no further improvement of the performance can be obtained by changing that particular N_i (i.e., reducing it) and its value is locked at the previous value.

The outer-loop iterates the operation of the inner-loop until all of the N_i's are either locked or have a value of 1; at this point, no further improvement of the performance is possible through changing any of the N_i's so that the stationary point has been obtained. Finally, the N_i's are summed and the constraint equation (Eq. 2.3-5) is used to compute the proper value of T_s. The algorithm shown in Fig. 2.4-1 is a gradient-like minimum-seeking algorithm with prescribed step sizes; i.e., integer changes in the N_i's.

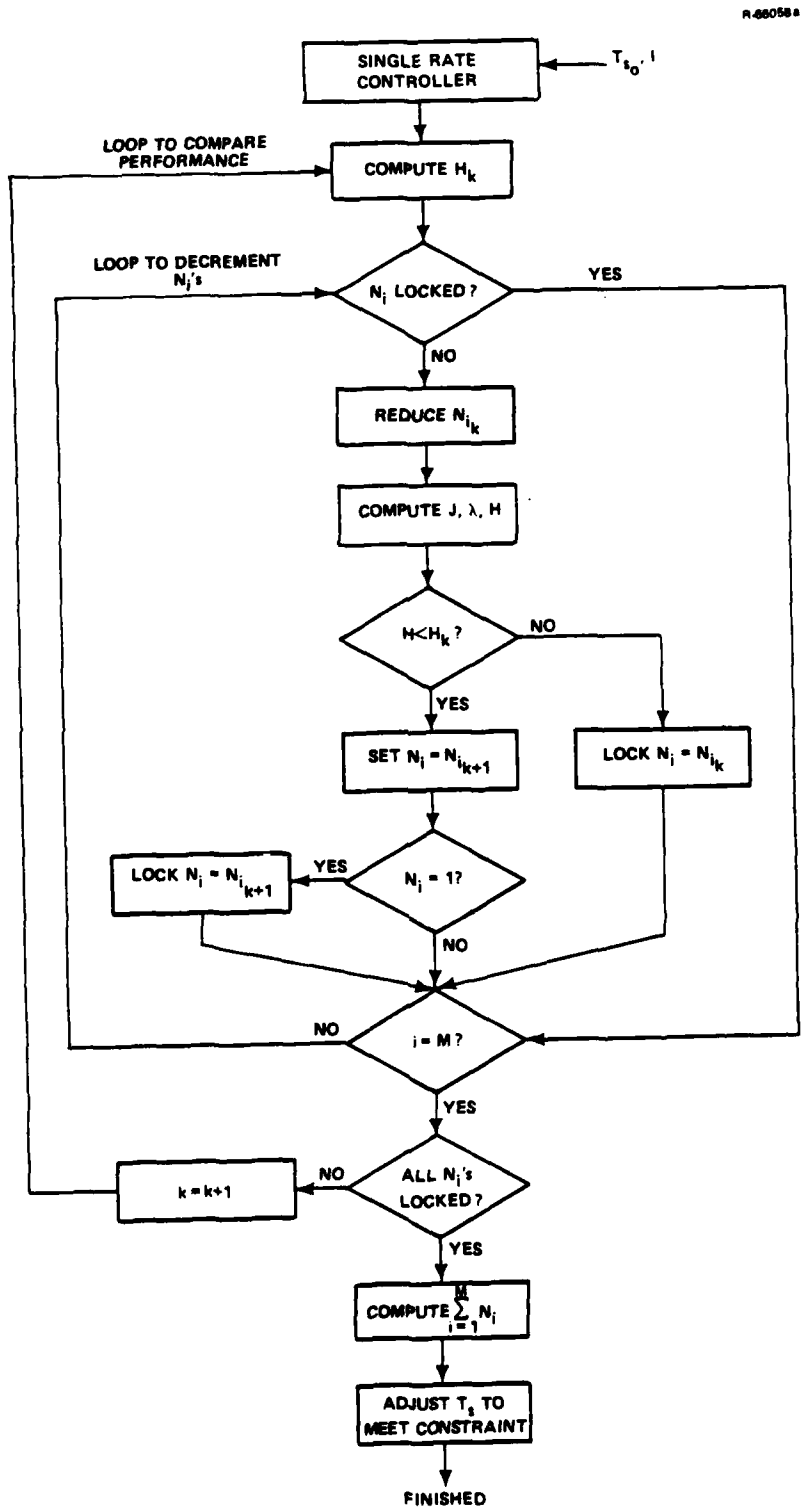

Figure 2.4-1 Optimization Algorithm

Computation of the Lagrange multiplier used in the optimization algorithm requires two related auxiliary computations:

- The sensitivity of the state error covariance with respect to T_s
- The sensitivity of the closed-loop dynamics with respect to T_s.

The sensitivity of the state error covariance is derived by differentiating the covariance equation with respect to T_s. The covariance equation, which has a periodic solution in steady-state, is given by:

$$P_{k+1} = \bar{\theta}_k P_k \bar{\theta}_k^T + Q_D \quad ; \quad k = 1,2,\ldots,\ell \tag{2.4-1}$$

where

$$\bar{\theta}_k = \Phi - \Gamma_k C_k = (I - \Gamma_k L_k)\theta_k \tag{2.4-2}$$

$$\theta_k = \Phi - \Gamma_k \hat{R}_k^{-1} \hat{M}_k \tag{2.4-3}$$

Differentiating Eq. 2.4-1, the covariance sensitivity is governed by:

$$\frac{\partial P_{k+1}}{\partial T_s} = \bar{\theta}_k \frac{\partial P_k}{\partial T_s} \bar{\theta}_k^T + \frac{\partial \bar{\theta}_k}{\partial T_s} P_k \bar{\theta}_k^T + \bar{\theta}_k P_k \frac{\partial \bar{\theta}_k^T}{\partial T_s} + \frac{\partial Q_D}{\partial T_s} \tag{2.4-4}$$

with

$$\frac{\partial \bar{\theta}_k}{\partial T_s} = (I - \Gamma_k L_k) \frac{\partial \theta_k}{\partial T_s} + \left[\frac{\partial}{\partial T_s} (I - \Gamma_k L_k)\right] \theta_k \tag{2.4-5}$$

Equation 2.4-4 is a periodic Liapunov equation with dynamics ($\bar{\theta}_k$) corresponding to the closed-loop system and forcing terms related to the sensitivity of the closed-loop dynamics ($\frac{\partial \bar{\theta}_k}{\partial T_s}$). Once a (periodic) solution to Eq. 2.4-4 has been obtained, the Lagrange multiplier is computed from:

$$\lambda = -\left(\frac{1}{\ell} \sum_{k=1}^{\ell} W_k \frac{\partial P_k}{\partial T_s} W_k^T\right) \left(\frac{f_c}{n t_m}\right)^{-1} \qquad (2.4\text{-}6)$$

The sensitivity of the closed-loop dynamics, required to compute the covariance sensitivity (and, hence, the Lagrange multiplier and Hamiltonian), is derived by differentiating the control solution Ricatti equation with respect to T_s. The Ricatti equation is given by:

$$K_k = \bar{\theta}_k^T K_{k+1} \bar{\theta}_k + L_k^T \hat{R}_k L_k + Q_k^* \qquad (2.4\text{-}7)$$

with

$$L_k = (\Gamma_k K_{k+1} \Gamma_k^T + \hat{R}_k)^{-1} \Gamma_k^T K_{k+1} \qquad (2.4\text{-}8)$$

Differentiating Eq. 2.4-7 one obtains (after algebra covered in Appendix A):

$$\frac{\partial K_k}{\partial T_s} = \bar{\theta}_k^T \frac{\partial K_{k+1}}{\partial T_s} \bar{\theta}_k + \bar{\theta}_k^T K_{k+1} \left(\frac{\partial \theta_k}{\partial T_s} - \frac{\partial \Gamma_k}{\partial T_s} L_k \theta_k\right) + \left(\frac{\partial \theta_k}{\partial T_s} - \frac{\partial \Gamma_k}{\partial T_s} L_k \theta_k\right)^T K_{k+1} \bar{\theta}_k$$

$$+ \frac{\partial Q_k^*}{\partial T_s} + \theta_k^T L_k^T \frac{\partial \hat{R}_k}{\partial T_s} L_k \theta_k \qquad (2.4\text{-}9)$$

Equation 2.4-9 is a periodic Liapunov equation with dynamics corresponding to the closed-loop system and forcing terms related to the derivatives of various plant dynamics matrices and design weighting matrices. The (periodic) solution of Eq. 2.4-9 is used to compute the sensitivity of the closed-loop dynamics matrix $(\frac{\partial \bar{\theta}_k}{\partial T_s})$ required to determine the error covariance sensitivity.

In this section an optimization algorithm for selecting sample rates of a multirate digital control system has been described. In the following section, this algorithm is applied to a prototype problem.

2.5 PROTOTYPE PROBLEM

In this section, the optimal sample rate selection approach developed in Sections 2.3 and 2.4 is demonstrated on a prototype problem: a lateral controller for the Space Shuttle Orbiter. A description of the prototype is given in Section 2.5.1; a demonstration of the optimization technique for this example is presented in Section 2.5.2; the effects of restricted computational budget and practical design considerations that arise from the observed effects are discussed in Section 2.5.3. The prototype investigation is summarized in Section 2.5.4.

2.5.1 System Description

The plant to be controlled is the lateral dynamics of the Space Shuttle Orbiter linearized about a re-entry flight condition:

$$\dot{\underline{x}} = F\underline{x} + G_f\delta_a + G_s\delta_r + \Lambda\underline{w} \qquad (2.5\text{-}1)$$

$$\underline{x}^T = (v,\ r_b,\ p_b,\ \Phi) \tag{2.5-2}$$

$$= (\text{sideslip velocity, yaw rate, roll rate, roll angle}) \tag{2.5-3}$$

$$\delta_a = \text{aileron deflection} \tag{2.5-4}$$

$$\delta_r = \text{rudder deflection} \tag{2.5-5}$$

$$\underline{w} = \text{white noise turbulence} \tag{2.5-6}$$

$$E\ \{\Lambda \underline{w}(t+\tau)\underline{w}(t)\Lambda\} = Q_c\delta(\tau) \tag{2.5-7}$$

The values of the various system matrices: F, G_f, G_s, Λ and Q_c are presented in Appendix B. It is worthwhile to note that the turbulence model used in this example forces the roll rate dynamics only; i.e., Q_c is of the form

$$Q_c = \begin{bmatrix} 0 & 0 & 0 & 0 \\ 0 & 0 & 0 & 0 \\ 0 & 0 & q_p & 0 \\ 0 & 0 & 0 & 0 \end{bmatrix} \tag{2.5-8}$$

The deterministic specifications of the continuous-time regulator (from which the multirate designs are derived), in terms of its closed-loop eigenvalues, are:

Roll-Spiral Dynamics:

$$s = -0.632 \pm i\ 0.913\ (\omega_o = 1.11 \text{ rad/sec},\ \xi = 0.569) \tag{2.5-9}$$

Dutch Roll Dynamics:

$$s = -0.522 \pm i\ 0.159\ (\omega_o = 0.546 \text{ rad/sec},\ \xi = 0.957) \tag{2.5-10}$$

The continuous-time control and state weighting matrices, R and Q, used to design the continuous-time regulator and to derive the multirate weighting matrices are presented in Appendix B.

The error rejection functional used in the present example is the average roll angle covariance over the ℓ cycle control period:

$$J = \frac{1}{\ell} \sum_{k=1}^{\ell} W_k P_k W_k^T \qquad (2.5\text{-}11)$$

with

$$W_k = (0, 0, 0, 1)$$

$$J = \frac{1}{\ell} \sum_{k=1}^{\ell} P_{44_k} \qquad (2.5\text{-}12)$$

With this choice of error rejection functional, the sample rate selection technique determines the sampling policy that minimizes the mean-square deviation from wings-level flight caused by the turbulence under a computational constraint.

The control period, ℓ, and computational budget, f_c/nt_m, for this example are:

$$\ell = 8 \qquad (2.5\text{-}13)$$

$$\frac{f_c}{nt_m} = 6.25/\text{sec} \qquad (2.5\text{-}14)$$

The value for ℓ was chosen to limit potential implementation complexity; i.e., the control schedule should not cover a large number of cycles. The computational budget parameters, Eq. 2.5-14, were chosen to illustrate "interesting" multirate optimization results. It should be mentioned that the budget chosen

is much tighter than that used in the operational Shuttle vehicle; the base sample rate derived in the subsequent computations is roughly five times lower than that of the operational Shuttle.

In this example, the goal of the optimization is to determine the base sample period, T_s, and rudder computation rate, N_r, to minimize J (as given by Eq. 2.5-12) under the computational constraint specified by Eq. 2.5-14. The aileron computation rate, N_a, is held constant at 8 (i.e., aileron is computed every base sample period). The results of this optimization are presented in the following subsection.

2.5.2 Optimization Results

Demonstration of the sample rate selection technique described in Section 2.3 using the prototype problem defined in Section 2.5.1 is presented here. For illustrative purposes, a survey of the payoff set (i.e., values of the error rejection functional over a range of values of the independent variables, T_s and N_r) is presented in Fig. 2.5-1. The surface* of the payoff set is smooth, displaying no local minimums that might "hang-up" a minimum seeking algorithm. The error rejection function is seen to monotonically increase with T_s and monotonically decrease with N_r (recall that as N_r increases the sample frequency for the rudder increases); the behavior of the error rejection functional makes sense in light of similar behavior in single rate digital systems (Ref. 5).

The locus of the constraint function (i.e., permissible combinations of T_s and N_r under the computational constaint)

*Although it is shown as such in Fig. 2.5-1, the payoff set is not a continuous surface. The payoff set is comprised of a set of curves for fixed integer values of N_r.

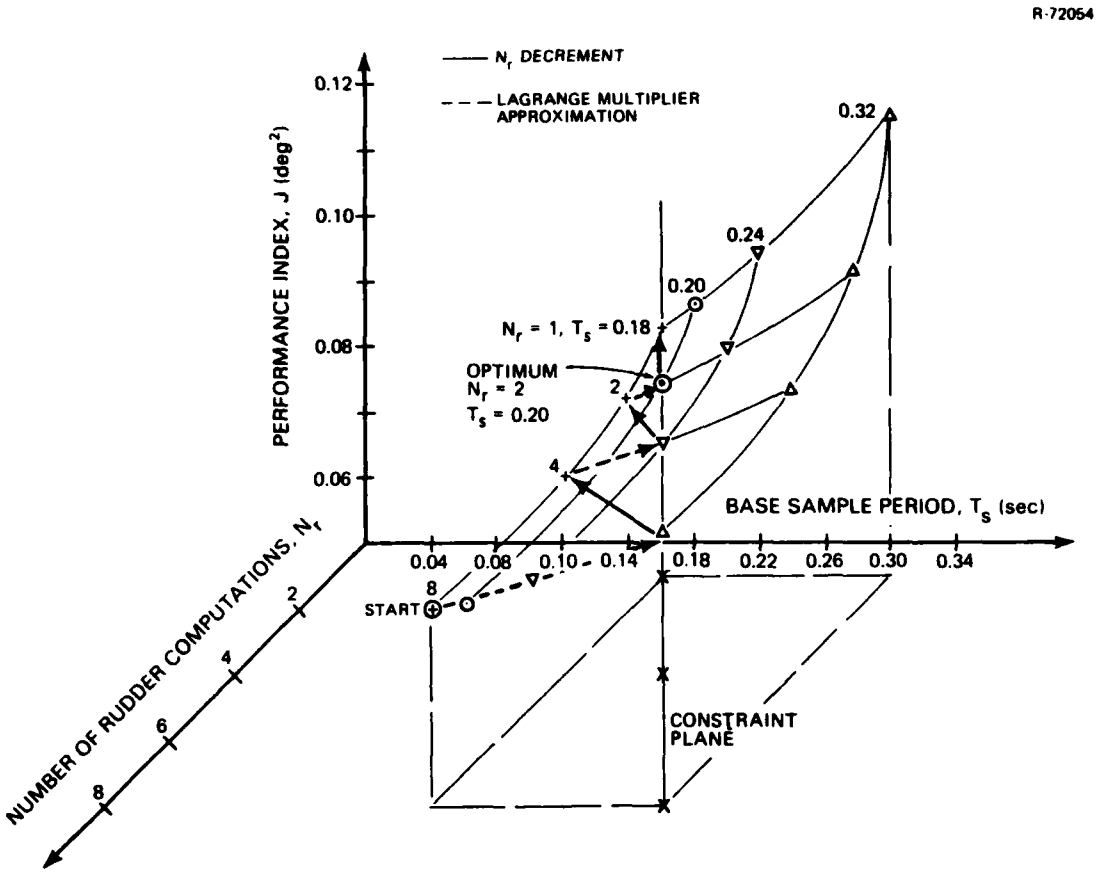

Figure 2.5-1 Optimal Sample Rate Selection for Space Shuttle Example

forms a plane in the [T_s, N_r, J] coordinate system. The intersection of the constraint plane with the performance "surface" is the payoff set of interest; the optimum error rejection under the computational constraint is located on this intersection.

The method of stepping-along the payoff/constraint intersection is illustrated in Fig. 2.5-1. As described in Section 2.3, the values of performance, J, along the payoff/constraint intersection are derived (approximately) by computing the Hamiltonian along the T_s = 0.18 sec plane and interpreting it as a gradient-projection of the performance function

from the T_s = 0.18 sec plane (with N_r fixed) to the C=0 plane. This gradient projection of the performance function is indicated by the dotted arrows in Fig. 2.5-1. The actual minimum-seeking is achieved by step-by-step decrementation of N_r (starting with a single rate system, N_r = 8) and comparison of the Hamiltonian function for each successive trial value of N_r. In proceeding to a new trial value of N_r, if the Hamiltonian is larger than that for the previous value of N_r, then the optimum has been overstepped, and the stationary point is deduced to be the previous value of N_r.

The stationary point for this case was determined to be at (N_r = 2, T_s = 0.18) as indicated in Fig. 2.5-1. The optimum and its neighboring points on the payoff/constraint intersection are shown in Fig. 2.5-2.

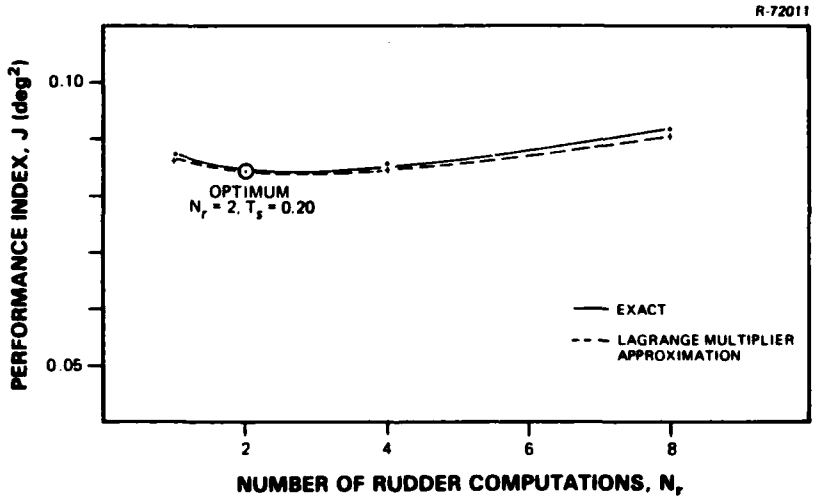

Figure 2.5-2 Performance Function in C=0 Plane for Prototype Problem

As shown in Fig. 2.5-2, there is a gradual improvement of performance from N_r = 8 down to the optimum at N_r = 2 followed by a significant increase in the performance function (for the small decrease in N_r) at N_r = 1. Also illustrated in Fig. 2.5-2

is the good agreement between the exact values of the performance function and those derived from the gradient projection for this case. In the following section, the effects of variations in computational budget (reduction of the computational budget in particular) on the optimal solution and resulting closed-loop system properties is investigated.

2.5.3 Limitations of the Gradient Algorithm

In the example of the previous section, there is good agreement of the exact performance and the approximate performance via the two-term Hamiltonian expression. When the budget is tightened (f_c/nt_m reduced), the Hamiltonian may not provide a good projection onto the constraint, C=0, plane.

The effects of a restricted computation budget are illustrated in Fig. 2.5-3. The computation budget has been reduced by a factor of four over the previous case (Section 2.5.2). The performance function in the C=0 plane as a function of rudder computation rate, N_r, is shown in Fig. 2.5-3. There is a sharp optimum, as indicated by the exact performance, in this case. The performance is relatively insensitive to N_r for values of 4 and 8; with N_r less than 4 (i.e., N_r equal to 2 or 1) there is a rapid degradation of performance. The Lagrange multiplier approximation is inaccurate for N_r=4 and N_r=8, causing the gradient-search algorithm to incorrectly select N_r=8 as the optimum when the actual optimum is at N_r=4.

Figure 2.5-4 shows the payoff set in the N_r=8 plane along with the gradient projection onto the C=0 plane. For the example illustrated in Fig. 2.5-4, the extrapolated value of J at C=0 is a poor approximation of the actual performance due to the curvature of the payoff set between the computation point (C=0.72) and the constraint plane (C=0).

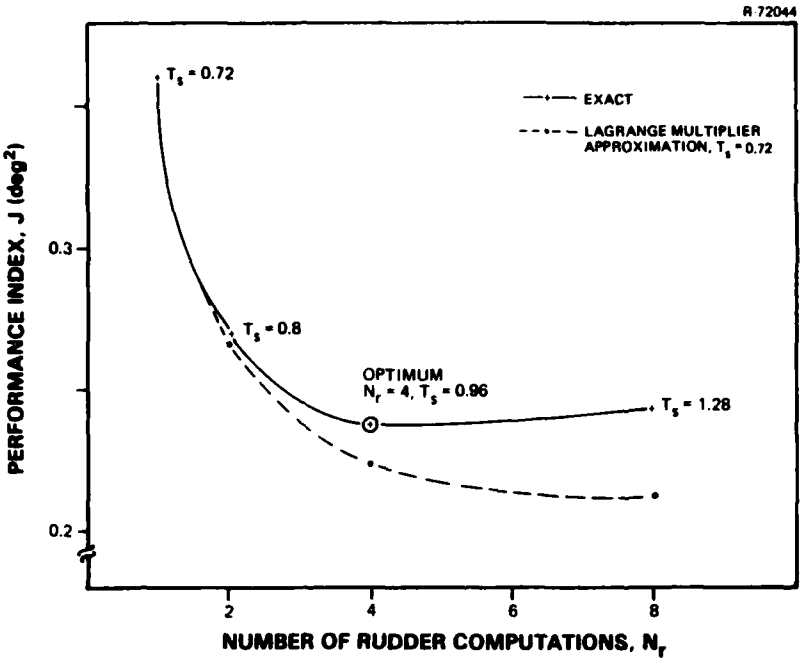

Figure 2.5-3 Payoff Set With Reduced Budget

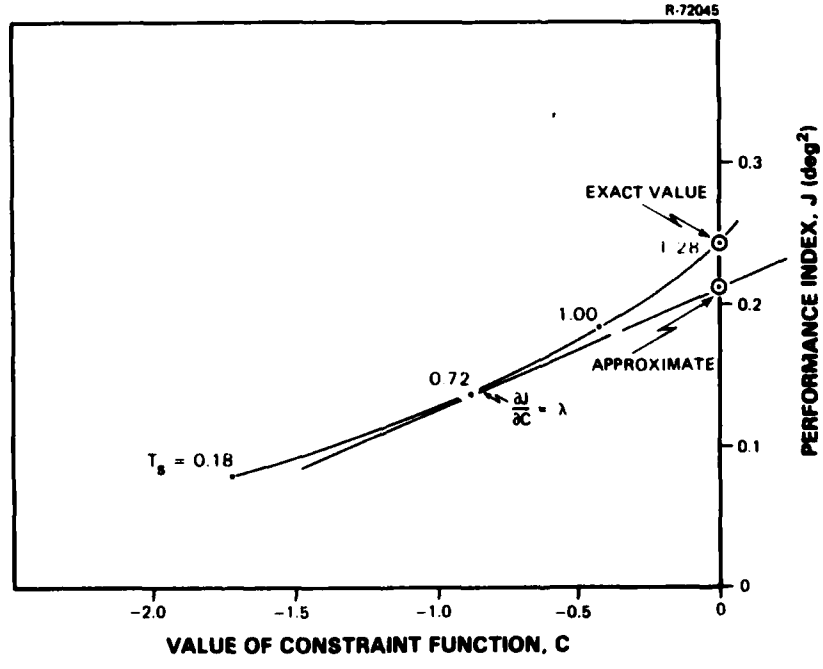

Figure 2.5-4 Payoff Set in N_r=8 Plane

There are many possible approaches that can be taken to obtain an improved projection of performance onto the constraint plane. One such approach would be to use a three-term "Taylor Series" approximation of the form;

$$J_o = J + \lambda \Delta C + \frac{1}{2} \frac{\partial \lambda}{\partial C} \Delta C^2 \qquad (2\text{-}4\text{-}15)$$

where $\frac{\partial \lambda}{\partial C}$ is derived by computing λ at two values of T_s and using a finite difference approximation.

Another approach is to use a successive approximation method whereby C is selected according to a modified Newton procedure:

$$C_{n+1} = -C_n + \frac{(H_n - J_n)}{p\lambda_n} \qquad (2.4\text{-}16)$$

where p is selected to reduce the extrapolation interval to the C=0 plane. For the case of p=2, C_{n+1} halves the interval to the C=0 plane; thus, determination of H_{n+1} would result in an improved approximation of J_o.

Use of the successive approximation technique with p=2 is shown in Fig. 2.5-5. An improved Hamiltonian approximation is obtained with the interval to the C=0 plane reduced. The successive approximation technique requires evaluation of J and λ at an additional point; thus, the gradient algorithm would require modification to include this additional computation.

At this point, some practical design issues related to optimal sample rate selection can be addressed:

- Reduced budget entails a larger base sample period and, hence, overall degradation of closed-loop performance

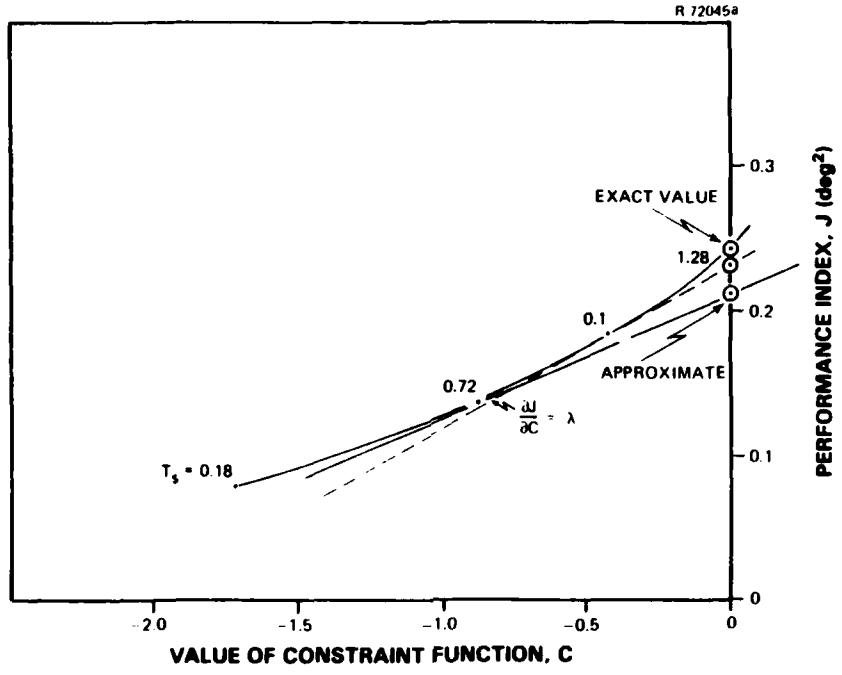

Figure 2.5-5 Successive Approximation of Performance

- Reduced budget may result in a controller having high sensitivity to parameter variations (as suggested by the curvature of the payoff set)
- The designer should apply judgement in using the optimal solution when high sensitivity (i.e., a sharp optimum) is indicated.

In comparing Figs. 2.5-3 with 2.5-2, an overall degradation of performance is observed for the restricted budget case owing to its longer base sample period. The sharp optimum evidenced in Fig. 2.5-3 suggests high system parameter sensitivity; the rapid degradation of performance for reduced rudder sample rates (reduced N_r) suggests that at the optimum, large changes in performance may result from relatively small changes in the design model parameters. In view of potential sensitivity of

the optimal performance, the designer should consider implementing a suboptimal sampling policy having lower sensitivity. For example, in Fig. 2.5-3, [N_r=8, T_s=1.28 sec] may be the preferred sample policy for implementation since it should be less sensitive to system parameter changes.

2.6 CHAPTER SUMMARY

In this chapter the problem statement, mathematical formulation, and solution procedure for selecting sample rates for multirate control systems is presented. The sample rate selection technique optimizes the disturbance rejection properties of the multirate controller under a computational constraint; an equivalent unconstrained optimization problem is derived by a Lagrange multiplier technique and a gradient-like algorithm to solve the optimization problem is described and demonstrated through a prototype problem.

The gradient-like optimization algorithm uses a Taylor series interpretation of the Hamiltonian function to project the error rejection performance from a trial point (where the computational constraint may not be satisfied) to the value of the base sampling period, T_s, that satisfies the computational constraint. The algorithm operates by systematically stepping in permissible integer values of the slow control sample rates to find the minimum of the performance function while satisfying the specified computational constraint.

The sample rate selection technique is demonstrated through a prototype problem. With a reasonable computation budget, an optimal base sample period and slow control sample rate are derived; error rejection performance computed by the Lagrange multiplier approximation and the exact performance

are in close agreement for this case. With a highly restricted computational budget, a strong optimum is obtained and poor agreement of the approximate performance and exact performance is observed. Modifications to the optimization algorithm to improve performance projection are outlined and practical considerations in using the derived sampling policy in implementation are discussed.

Again, the deterministic design procedure (reported in Ref. 1 and summarized in Section 2.1) along with the sample rate selection technique described in this chapter allow the designer to optimize the disturbance-rejection properties of the controller under a computational constraint while maintaining desirable transient response characteristics. Specifically, the flight control engineer can select a control computation schedule to optimize the rejection of disturbances (principally from turbulence) while the maintaining specified handling qualities and satisfying computational constraints.

3. EXAMPLE SYSTEM DESIGN

3.1 OVERVIEW

In this chapter the sample rate optimization formulation developed in Chapter 2 is applied to a practical flight control system example. A dynamic model of a Navy fighter aircraft with a multirate control system structure is developed. With an appropriate computational constraint and performance function defined, the optimal sampling policy of the multirate system is selected. The performance and properties of the optimum system are investigated as a function of flight condition.

3.2 MATHEMATICAL FORMULATION

3.2.1 Aircraft/Disturbance Dynamics

Figure 3.2-1 is a block diagram of the example aircraft/disturbance/controller model. The plant to be controlled is the longitudinal dynamics of the F-14 aircraft in trimmed level flight. The dynamics of the vehicle are disturbed by atmospheric turbulence; the turbulence model used in the present example is derived from the Dryden turbulence spectra (Ref. 6). The aircraft is regulated about its nominal level-flight condition by a multirate proportional-plus-integral controller.

The open-loop continuous-time aircraft/disturbance dynamics are given by:

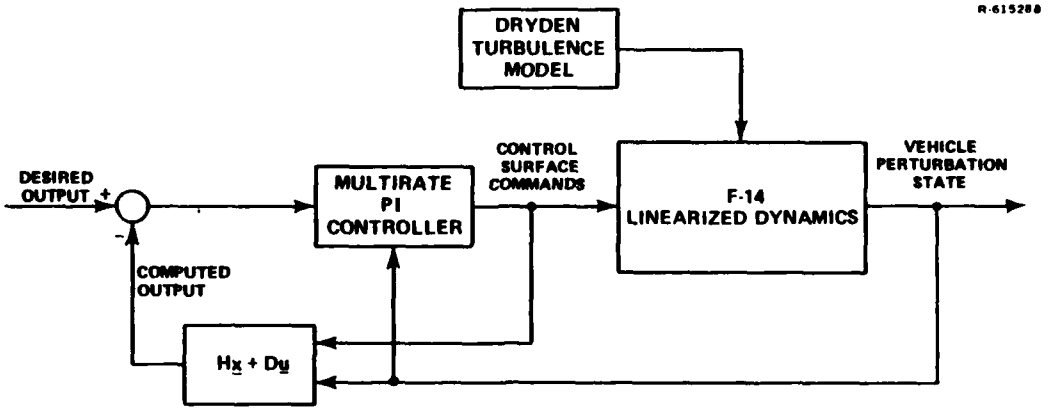

Figure 3.2-1 Aircraft Example Models

$$\dot{\underline{x}} = F\underline{x} + G\underline{u} + \Lambda_d w \qquad (3.2\text{-}1)$$

where,

$$\underline{x}^T = (\theta, u, q, w, w_g, x_2)$$

= (pitch attitude, forward velocity, pitch rate, vertical velocity, vertical velocity component of turbulence, auxiliary turbulence state)

$$\underline{u}^T = (\delta_e, \delta_{mf})$$

= (elevator, maneuver-flap)

$$w \sim N(0,1)$$

The matrices that define the dynamic model of Eq. 3.2-1 are:

$$F = \begin{bmatrix} \tilde{F} & \tilde{F}_c \\ 0 & F_d \end{bmatrix} \qquad (3.2\text{-}2)$$

$$G = \begin{bmatrix} \tilde{G} \\ 0 \end{bmatrix} \qquad (3.2\text{-}3)$$

$\tilde{F}$ = vehicle longitudinal dynamics

$$\tilde{F}_c = \begin{bmatrix} 0 & 0 \\ \underline{f}_w - \frac{\beta}{V}\underline{f}_q & \frac{\beta}{V}\underline{f}_q \end{bmatrix} \qquad (3.2\text{-}4)$$

$$F_d = \begin{bmatrix} -\beta & \beta \\ 0 & -\beta \end{bmatrix} \qquad (3.2\text{-}5)$$

$$\Lambda_d = \begin{bmatrix} \frac{1}{V}\sqrt{3\beta} & \beta & \underline{f}_q \\ \sqrt{3\beta} & \beta & \\ \sqrt{2\beta} & \beta & \end{bmatrix} \sigma_w \qquad (3.2\text{-}6)$$

The augmented system defined by Eqs. 3.2-1 to 3.2-6 is derived by coupling the turbulence model dynamics to the aircraft dynamics. The dynamics matrix, F, is comprised of blocks related to the aircraft dynamics ($\tilde{F}$), the disturbance dynamics (F_d), and the aerodynamic coupling between the disturbance and the aircraft ($\tilde{F}_c$). The column vectors, $\underline{f}_w$ and $\underline{f}_q$, are derived from the third and fourth columns of $\tilde{F}$ and represent the aerodynamic couplings of turbulence velocities into vehicle motion. The scalar, β, is related to the temporal bandwidth of the turbulence model and is derived from:

$$\beta = \frac{V}{L_w} \qquad (3.2\text{-}7)$$

where

V = aircraft nominal airspeed

L_w = spatial scale of Dryden turbulence model

The continuous-time dynamics given by Eq. 3.2-1 are converted to discrete-time by the procedure described in Section 2.1. Numerical values of the various system matrices are given in Appendix C.

3.2.2 Control System

The controller used in this example is a multirate proportional-plus-integral (PI) controller designed to the same deterministic specifications as the F-14 control system studied in Ref. 7. The gradient-search algorithm is used to determine the optimal disturbance rejection of the closed-loop system and corresponding sample rates. Since, in this example, the controller is to maintain trimmed level flight as accurately as possible, it is implemented in its type 0 form; the feedback variable transformation to obtain a pure integration in the forward control path (Ref. 1) is not performed.

The controller deterministic specifications are embodied in the elements of the (continuous-time) quadratic cost-functional matrices. The weighting matrices in the present example are generated by specifying maximum values for the various state, control, control rate, and output variables and using the following formulae to relate these design parameters to the states and controls of the (augmented) system:

$$Q = \left[\begin{array}{c|c} \dfrac{1}{\Delta x^2_{\max\, i}} & 0 \\ \hline 0 & \dfrac{1}{\Delta u^2_{\max\, i}} \end{array}\right] + \begin{bmatrix} \tilde{F}^T \\ G^T \end{bmatrix} \left[\frac{1}{\Delta \dot{x}^2_{\max\, i}}\right] \begin{bmatrix} \tilde{F} & \tilde{G} \end{bmatrix}$$

$$+ \begin{bmatrix} H_x^T \\ H_u^T \end{bmatrix} \left[\frac{1}{\Delta y^2_{\max\, i}}\right] \begin{bmatrix} H_x & H_u \end{bmatrix} \qquad (3.2\text{-}8)$$

$$R = \left[\frac{1}{\Delta u^2_{max\ i}}\right] \qquad (3.2\text{-}9)$$

where

$$A = [z_i]$$

indicates a diagonal matrix with

$$A_{ii} = z_i$$

and

$\Delta x_{max\ i}$ = maximum value of vehicle state variable i

$\Delta u_{max\ i}$ = maximum value of control variable i

$\Delta \tilde{x}_{max\ i}$ = maximum value of state variable i derivative

$\Delta \dot{u}_{max\ i}$ = maximum value of control variable i rate

$\Delta y_{max\ i}$ = maximum value of vehicle output variable i

The maximum values used in the present example are listed in Table 3.2-1. The multirate controller weighting matrices are computed by the design-to-specification procedure described in Section 2.1. The control system implementation is given by:

$$\underline{u}_k = -C_{1_k}\,\underline{x}_{k-1} + (I - T_s C_{2_k})\,\underline{u}_{k-1} + T_s\,C_{3_k}\,\underline{v}_{s_k} \qquad (3.2\text{-}9)$$

where $\underline{v}_{s\ k}$ is the slow control (maneuver flap) increment computed at an integer multiple of the base sample period. The gains -- C_{1_k}, C_{2_k}, C_{3_k} -- are computed from the solution of the periodic Ricatti equation corresponding to each trial control computation schedule.

TABLE 3.2-1
CONTROL SYSTEM VARIABLE WEIGHTS

MATRIX	MATRIX TYPE	VARIABLE NAME	MAXIMUM VALUE
Q	Vehicle State	Pitch Angle, θ	10 deg
		Axial Velocity, u	5 ft/sec
		Pitch Rate, q_b	20 deg/sec
		Vertical Velocity, w	25 ft/sec
Q	Vehicle Control	Elevator Deflection, δ_e	5 deg
		Maneuver Flap Deflection, δ_{mf}	∞
Q	State Derivative	Pitch Angle, $\dot{\theta}$	∞
		Axial Acceleration, $\dot{U}$	25 ft/sec^2
		Pitch Acceleration, $\dot{q}_b$	∞
		Vertical Acceleration, $\dot{w}$	∞
Q	Output	Normal Acceleration, a_n	3 ft/sec^2
		Maneuver Flap Deflection, δ_{mf}	5 deg
R	Control Rates	Elevator Rate	3 deg/sec
		Maneuver Flap Rate	6 deg/sec

3.2.3 Performance Function and Computational Constraint

The steady-state variance of the vehicle normal acceleration at the vehicle center of gravity, a_n, in response to vertical turbulence is chosen as the performance function; the physical environment corresponding to this choice of performance index is depicted in Fig. 3.2-2. Normal acceleration is an appropriate measure of vehicle/control system performance on physical grounds in that it is closely related to ride quality standards (see Refs. 8 and 9, for example). Maintaining vertical accelerations at acceptable low-levels is an important control function with respect to preventing pilot fatigue and, possibly, motion sickness.

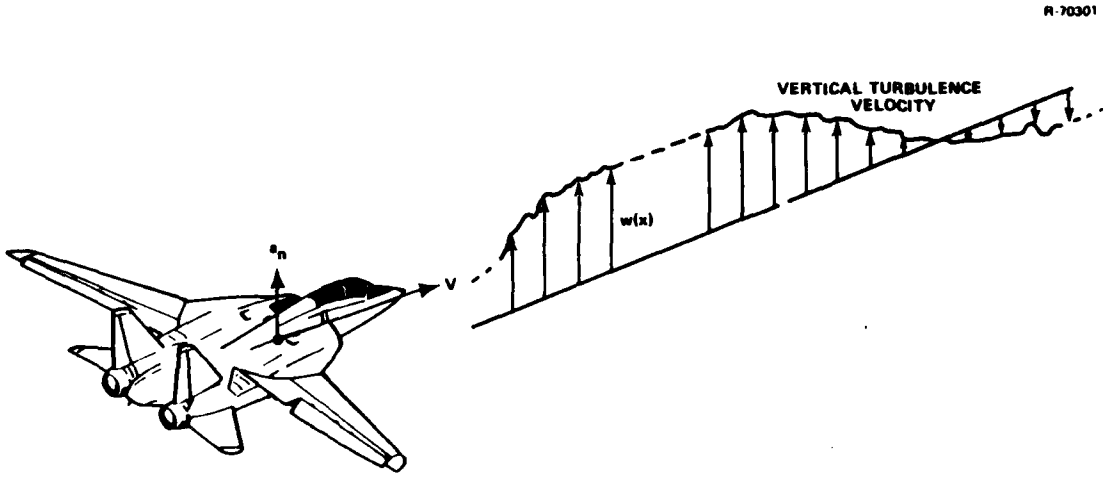

Figure 3.2-2 Flight Condition and Performance Function for the Example

Mathematically the error rejection performance function is defined by:

$$J = E\{a_n^2\} \tag{3.2-12}$$

$$= \frac{1}{\ell} \sum_{k=1}^{\ell} W_k P_k W_k^T \tag{3.2-13}$$

with

$$a_n = Vq - \dot{w} \tag{3.2-14}$$

where

P_k = steady-state covariance matrix of the closed-loop system

W_k = weighting array

ℓ = control schedule period

V = nominal airspeed

and $E[\cdot]$ is the expectation operator.

The elements of the weighting array, W_k, are derived from Eq. 3.2-14 using the vehicle state equation for $\dot{w}$, i.e.,:

$$\dot{w} = \tilde{f}\underline{x} + \tilde{g}\underline{u} \tag{3.2-15}$$

$$a_n = W_k \begin{bmatrix} \underline{x} \\ --- \\ \underline{u} \end{bmatrix} \tag{3.2-16}$$

$$W_k = V(0,0,1,0,0,0,0,0) - (\tilde{f}\ \tilde{g}) \tag{3.2-17}$$

where $\tilde{f}$ and $\tilde{g}$ are the row elements of the F and G matrices (Eq. 3.2-1) which constitute the differential equation for w.

For this example, the computational constraint (Table 2.2-1) reduces to:

$$\frac{f_c T_s}{n t_m} - \frac{1}{\ell}(N_e + N_{mf}) = 0 \tag{3.2-18}$$

where

N_e = number of elevator control computations per ℓ cycle period

$= \ell$

N_{mf} = number of maneuver-flap computations per ℓ cycle period

The control period and computation budget are:

$$\ell = 8 \tag{3.2-19}$$

$$\frac{f_c}{nt_m} = 20.0/\text{sec} \qquad (3.2\text{-}20)$$

The control period value was chosen in consideration of implementation complexity; i.e., a control period longer than 8 cycles would entail involved logic in the software to "keep track of" the control schedule. The computation budget was chosen to achieve a 50 percent reduction of computation over a single-rate controller operating at a 20 Hz sample rate.

3.3 SAMPLE RATE SELECTION RESULTS

The results of the performance optimization for the F-14 example are presented in this section. Several flight conditions are chosen to determine system performance and sample rate sensitivities to variations in flight condition. Although an exhaustive survey of the entire F-14 flight envelope was not performed, it is possible to derive some useful conclusions from the flight conditions selected.

The error rejection performance of the aircraft in trimmed level flight at an altitude of 20,000 ft and an airspeed of 999 ft/sec is shown in Fig. 3.3-1. A strong optimum is evidenced compared to other flight conditions surveyed; the optimal sampling policy is $N_{mf} = 4$ and $T_s = 0.075$ sec. There is a slight reduction in mean square normal acceleration as N_{mf} is decreased from 8 to 4; further reduction in the number of maneuver-flap computations results in significant degradation of performance; thus, the maneuver-flap gust alleviation potential rapidly degrades at low sample rates ($N_{mf}<4$).

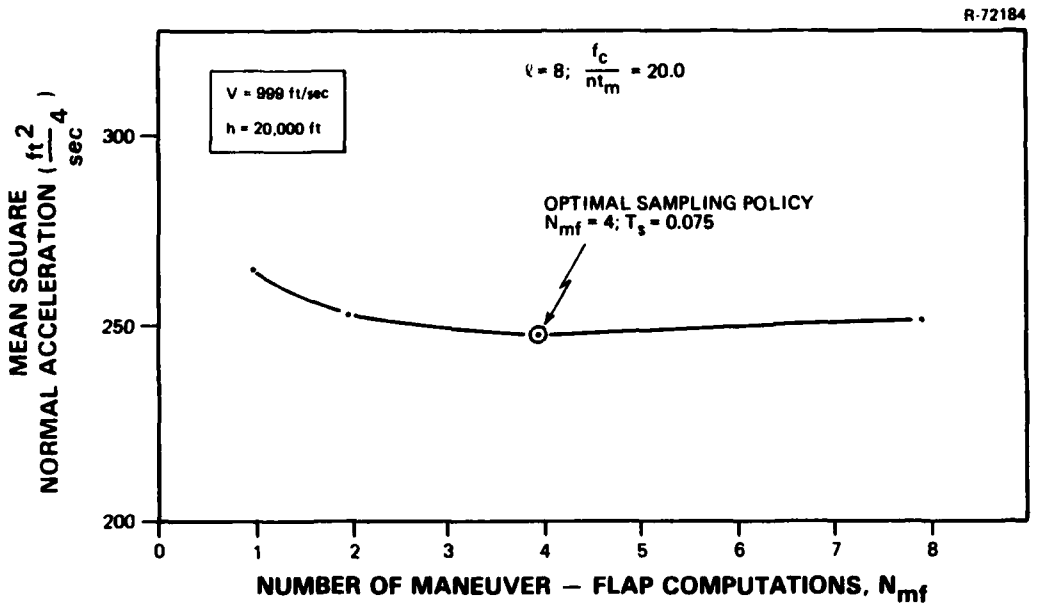

Figure 3.3-1 Performance Function for Example

The correlation coefficients for maneuver-flap and elevator against vertical velocity, $\rho_{w/\delta f}$ and $\rho_{w/\delta e}$, and against the vertical velocity turbulence component, $\rho_{\delta f/wg}$ and $\rho_{\delta e/wg}$, for different maneuver-flap computation rates are shown in Fig. 3.3-2(a), (b). The cross correlations rapidly drop off past the optimal ($N_{mf}<4$); this indicates that at low sample rates the flight control system loses its ability to track disturbance inputs due to the large time period between maneuver-flap updates.

The error rejection performance in trimmed level flight at an altitude of 20,000 ft and an airspeed of 400 ft/sec is shown in Fig. 3.3-3. For this flight condition, the performance is insensitive to sampling policy (i.e., the system exhibits a

R-76528

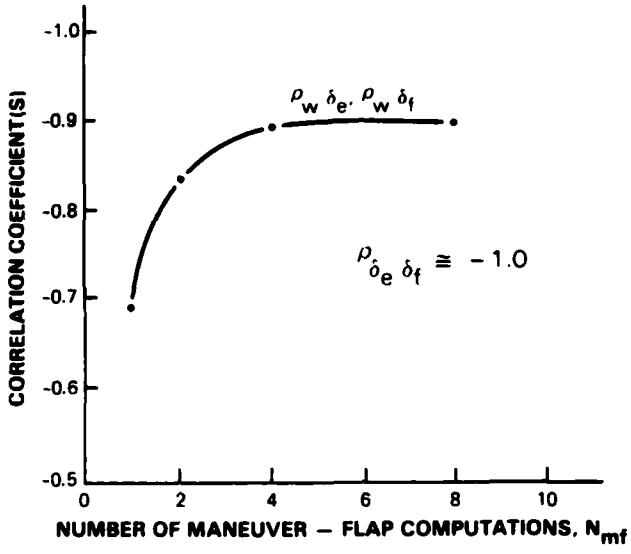

R-76529

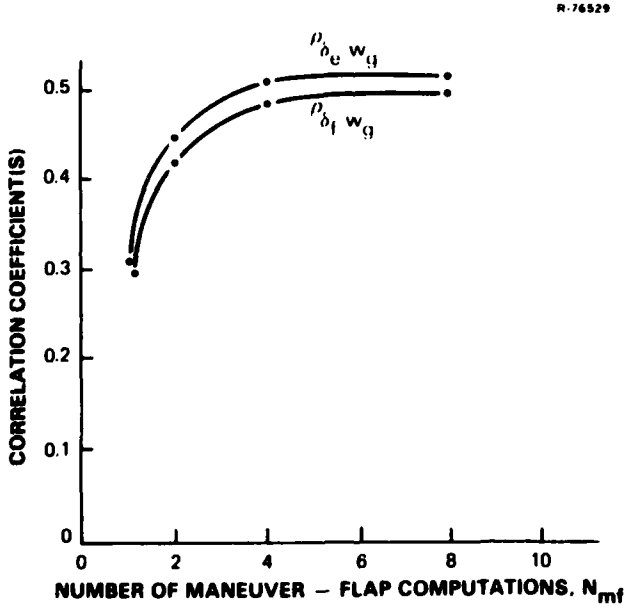

Figure 3.3-2 Correlation Coefficients for the Example

very weak optimum. The optimum occurs at $N_{mf} = 2$ and $T_s = 0.0625$ sec. The performance insensitivity to sampling policy illustrated in Fig. 3.3-3 indicates that a potential reduction in total computation time, due to reduced maneuver-flap sampling rate, can result from a multirate design; hence, multirate design offers a distinct computational advantage over single rate for this case.

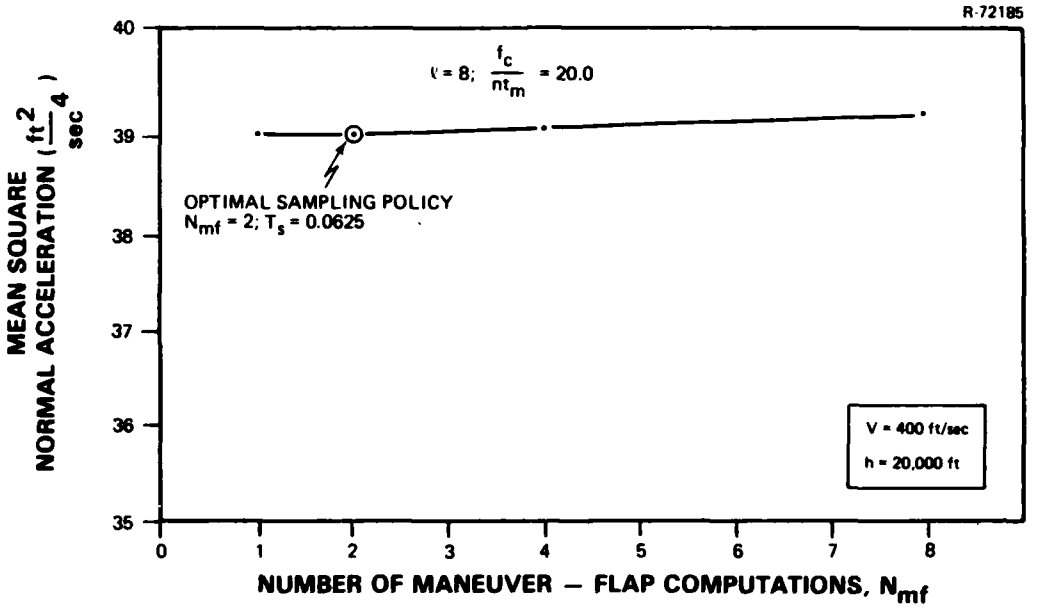

Figure 3.3-3 Performance Function at Second Flight Condition

A practical design procedure to derive a sampling policy to cover a complete flight coindition envelope can be conjectured at this point:

- Perform an exhaustive survey of optimal sampling policies as a function of flight condition over the vehicle operational envelope

- Determine the subset of flight conditions that exhibit strong optimums
- Choose a single control schedule that has minimal off-optimal performance degradation over the entire flight envelope.

In the present example, choice of the optimum schedule for 20,000 ft at 999 ft/sec would not result in significant performance degradation for the other flight condition surveyed (e.g., for h = 20,000 ft at v = 400 ft/sec, a suboptimal design would be acceptable due to low sensitivity)

3.4 CHAPTER SUMMARY

In this chapter, the sample rate selection procedure has been applied to an example aircraft: An F-14 that is "flown" through a vertical atmospheric disturbance. Steady-state variance of the closed-loop aircraft normal acceleration at the center-of-gravity is chosen as the performance index. The sample rate optimization problem for the case of a fixed computation budget is solved to determine the optimum choice of sample period, T_s, and maneuver-flap computation rate, N_{mf}.

Variations of the optimal solution as a function of flight condition were examined. It was found that about strong optimums there is a rapid drop-off of correlation between control action and disturbance input as the slow control sample rate is reduced. Other flight conditions surveyed show performance that is insensitive to sampling policy. A practical design procedure would be to perform an exhaustive survey of the entire flight envelope, to look for flight conditions having strong optimums, and to choose a control schedule based on the strong optimums.

4. CONCLUSIONS AND RECOMMENDATIONS

The net result of the present research (including that reported in Ref. 1) is a general technique for digital flight control design. Using the design-to-specification procedure, the designer is able to synthesize multirate digital controllers having uniform handling qualities (i.e., deterministic response) which are independent of the control schedule chosen (within the limitations of the sampling theorem). Using the sample rate selection procedure outlined in the present report, the disturbance rejection properties of the controller are optimized under a quantitative computational constraint (i.e., computer specifications and budget are included as design parameters). As a result of these two (automated) procedures, the designer can conveniently structure and design a control system entirely in continuous-time; conversion to a multirate digital implementation and selection of control sample rates to accommodate computational constraints is then achieved automatically.

4.1 CONCLUSIONS

The research reported in this document provides the following significant results:

- Formulation of the Optimal Sample Rate Selection Problem - The optimal sample rate selection problem is formulated as a constrained optimization problem and converted to an equivalent unconstrained problem by Lagrange multiplier techniques. General formulae for the error rejection performance functional and the computational constraint are presented; sufficient

conditions for a stationary point of the corresponding Hamiltonian function are derived.

- Optimization Algorithm - A gradient-like algorithm to solve the optimal sample rate selection problem is derived. This algorithm performs a step-by-step optimization of the cost functional moving in prescribed, integer-valued steps of the control sample rates. Limitations of the algorithm for highly constrained computation budgets are investigated; alternative measures to overcome these limitations are discussed.

- Example Application - The sample rate selection technique is applied to a practical design example: a flight control system for the F-14 aircraft. A physically-motivated performance measure, rms normal acceleration, is selected and quantitatively related to the general error rejection functional. Optimal control schedules are derived for a limited set of flight conditions; practical considerations for control schedule selection are made based on these results.

4.2 RECOMMENDATIONS

It is recommended that the following studies related to the present investigation be undertaken.

- Investigate the effects of control schedule on control system sensitivity to uncertain plant parameters. Determine appropriate parameter sensitivity metrics. Formulate and derive a solution methodology to optimize the sensitivity metric under a computational constraint. Investigate the properties of the optimal solution through a design example.

- Apply the techniques developed in the present research to a practical flight control system. Aeroelastic vehicle control design would be a particularly attractive test application.

- Investigate the application of multirate control/sample rate selection techniques to other areas of control; e.g., process control scheduling, multi-target tracking, remote-to-central packet switching schedule, and attention allocation/dynamic decision modeling in human operator applications.

APPENDIX A
COVARIANCE AND CONTROL SOLUTION SENSITIVITIES

Derivations of the covariance and control sensitivity equations (Eqs. 2.4-4 and 2.4-9, respectively) are presented here. The covariance sensitivity equation is derived in Section A.1; the control solution sensitivity is presented in Section A.2.

A.1 COVARIANCE SENSITIVITY

As discussed in Section 2.4, direct differentation of the covariance equation, Eq. 2.4-1, results in

$$\frac{\partial P_{k+1}}{\partial T_s} = \bar{\theta}_k \frac{\partial P_k}{\partial T_s} \theta_k^T + \frac{\partial \bar{\theta}_k}{\partial T_s} P_k \bar{\theta}_k^T + \bar{\theta}_k P_k \frac{\partial \bar{\theta}_k}{\partial T_s} + \frac{\partial Q_D}{\partial T_s} \qquad (2.4\text{-}4)$$

with

$$\frac{\partial \bar{\theta}_k}{\partial T_s} = (I - \Gamma_k L_k) \frac{\partial \theta_k}{\partial T_s} + \left[\frac{\partial}{\partial T_s} (I - \Gamma_k L_k)\right] \theta_k \qquad (2.4\text{-}5)$$

It is necessary to evaluate the first factor of the second term in Eq. 2.4-5:

$$\frac{\partial}{\partial T_s} (I - \Gamma_k L_k) = \frac{\partial}{\partial T_s} \left[I - \Gamma_k (\Gamma_k K_{k+1} \Gamma_k^T + \hat{R}_k)^{-1} \Gamma_k^T K_{k+1}\right] \qquad (A.1\text{-}1)$$

$$= \frac{\partial}{\partial T_s} (I + \Gamma_k \hat{R}_k^{-1} \Gamma_k^T K_{k+1})^{-1} \qquad (A.1\text{-}2)$$

Equation A.1-2 is a more convenient form for this derivation and was obtained using the matrix identity:

$$[I-Y^T(ZY^T+X)^{-1}Z] = (I+Y^TX^{-1}Z)^{-1} \qquad (A.1\text{-}3)$$

with

$$x = \hat{R}_k$$

$$y = z = \Gamma_k K_{k+1}^{1/2}$$

Carrying out the differentation in Eq. A.1-2 one obtains:

$$\frac{\partial}{\partial T_s}(I+\Gamma_k\hat{R}_k^{-1}\Gamma_k^T K_{k+1})^{-1} = -(I+\Gamma_k\hat{R}_k^{-1}\Gamma_k^T K_{k+1})^{-1}\frac{\partial}{\partial T_s}[(I+\Gamma_k\hat{R}_k^{-1}\Gamma_k^T K_{k+1})]$$

$$(I+\Gamma_k\hat{R}_k^{-1}\Gamma_k^T K_{k+1})^{-1} \qquad (A.1\text{-}4)$$

$$= -(I-\Gamma_k L_k)\frac{\partial}{\partial T_s}[(I+\Gamma_k\hat{R}_k^{-1}\Gamma_k^T K_{k+1})](I-\Gamma_k L_k)^T \qquad (A.1\text{-}5)$$

The matrix identity of Eq. A.1-3 was used again (in reverse) to derive Eq. A.1-5 from A.1-4. Carrying out the differentiation of the inner factor of Eq. A.1-5 one obtains:

$$\frac{\partial}{\partial T_s}(I-\Gamma_k L_k) = -(I-\Gamma_k L_k)\left\{\left[\frac{\partial\Gamma_k}{\partial T_s}\hat{R}_k^{-1}\Gamma_k^T+\Gamma_k\hat{R}_k\frac{\partial\Gamma_k}{\partial T_s} - \Gamma_k\hat{R}_k^{-1}\frac{\partial\hat{R}_k}{\partial T_s}\hat{R}_k^{-1}\Gamma_k^T\right]K_{k+1} + \Gamma_k\hat{R}_k^{-1}\Gamma_k\frac{\partial K_{k+1}}{\partial T_s}\right\}(I-\Gamma_k L_k)^T \qquad (A.1\text{-}6)$$

The remaining derivatives, $\frac{\partial \theta_k}{\partial T_s}$ and $\frac{\partial Q_D}{\partial T_s}$, are derived by straightforward differentiation:

$$\theta_k = \Phi - \Gamma_k \hat{R}_k^{-1} \hat{M}_k^T \tag{A.1-7}$$

$$\boxed{\frac{\partial \theta_k}{\partial T_s} = F\Phi - \frac{\partial \Gamma_k}{\partial T_s} \hat{R}_k^{-1} \hat{M}_k^T + \Gamma_k \hat{R}_k^{-1} \frac{\partial \hat{R}_k}{\partial T_s} \hat{R}_k^{-1} \frac{\partial \hat{M}_k^T}{\partial T_s} - \Gamma_k \hat{R}_k^{-1} \frac{\partial \hat{M}_k^T}{\partial T_s}} \tag{A.1-8}$$

$$Q_D = \int_0^{T_s} e^{Fs}(\Lambda\Lambda^T)(e^{Fs})^T \, ds \tag{A.1-9}$$

$$\boxed{\frac{\partial Q_D}{\partial T_s} = \Phi(\Lambda\Lambda^T)\Phi^T} \tag{A.1-10}$$

B.2 CONTROL SOLUTION SENSITIVITY

The control solution sensitivity is derived by direct differentiation of the discrete time Ricatti equation. Differentiation and algebraic reduction of the Ricatti equation is presented here.

$$K_k = \theta_k^T (I - L_k^T \Gamma_k^T) K_{k+1} \theta_k + Q_k^* \tag{A.2-1}$$

$$= \theta_k^T K'_{k+1} \theta_k + Q_k^* \tag{A.2-2}$$

where

$$K'_{k+1} = (I - L_k^T \Gamma_k^T) K_{k+1}$$

$$= K_{k+1}[I - \Gamma_k (\Gamma_k^T K_{k+1} \Gamma_k + R)^{-1} \Gamma_k^T K_{k+1}] \tag{A.2-3}$$

Differentiating Eq. A.2-2, one obtains

$$\frac{\partial K_k}{\partial T_s} = \theta_k^T \frac{\partial K_{k+1}}{\partial T_s} \theta_k + \frac{\partial \theta_k^T}{\partial T_s} K'_{k+1}\theta_k + \theta_k^T K'_{k+1} \frac{\partial \theta_k}{\partial T_s} + \frac{\partial Q_k^*}{\partial T_s} \tag{A.2-4}$$

The partial derivative of K'_{k+1} is derived by differentiating Eq. A.2-3.

$$\frac{\partial K'_{k+1}}{\partial T_s} = \frac{\partial K_{k+1}}{\partial T_s} (I-\Gamma_k L_k) - K_{k+1} \frac{\partial}{\partial T_s} \left[\Gamma_k(\Gamma_k^T K_{k+1}\Gamma_k+\hat{R}_k)^{-1}\Gamma_k^T K_{k+1}\right]$$

$$= \frac{\partial K_{k+1}}{\partial T_s} (I-\Gamma_k L_k) - K_{k+1} \frac{\partial \Gamma_k}{\partial T_s} L_k - K_{k+1} L_k^T \frac{\partial \Gamma_k^T}{\partial T_s}$$

$$- L_k^T \Gamma_k^T \frac{\partial K_{k+1}}{\partial T_s} + K_{k+1}\Gamma_k \frac{\partial}{\partial T_s} (\Gamma_k^T K_{k+1}\Gamma_k+\hat{R}_k)^{-1}\Gamma_k^T K_{k+1} \tag{A.2-6}$$

Now

$$\frac{\partial}{\partial T_s} (\Gamma_k^T K_{k+1}\Gamma_k+\hat{R}_k)^{-1} =$$

$$- (\Gamma_k^T K_{k+1}\Gamma_k+\hat{R}_k)^{-1} \left\{ \frac{\partial \Gamma_k^T}{\partial T_s} K_{k+1}\Gamma_k + \Gamma_k^T K_{k+1} \frac{\partial \Gamma_k}{\partial T_s} \right.$$

$$\left. + \Gamma_k^T \frac{\partial K_{k+1}}{\partial T_s} \Gamma_k + \frac{\partial \hat{R}_k}{\partial T_s} \right\} (\Gamma_k^T K_{k+1}\Gamma_k+\hat{R}_k)^{-1} \tag{A.2-7}$$

so that

$$\frac{\partial K'_{k+1}}{\partial T_s} = \frac{\partial K_{k+1}}{\partial T_s}(I-\Gamma_k L_k) - K_{k+1}\frac{\partial \Gamma_k}{\partial T_s}L_k - L_k^T\frac{\partial \Gamma_k}{\partial T_s}K_{k+1} - L_k\Gamma_k^T\frac{\partial K_{k+1}}{\partial T_s}$$

$$- L_k^T\left\{\frac{\partial \Gamma_k}{\partial T_s}K_{k+1}\Gamma_k + \Gamma_k^T K_{k+1}\frac{\partial \Gamma_k}{\partial T_s} + \Gamma_k^T\frac{\partial K_{k+1}}{\partial T_s}\Gamma_k + \frac{\partial \hat{R}_k}{\partial T_s}\right\}L_k$$

(A.2-8)

or

$$\frac{\partial K'_{k+1}}{\partial T_s} = (I-\Gamma_k L_k)\frac{\partial K_{k+1}}{\partial T_s}(I-\Gamma_k L_k) - (I-L_k^T\Gamma_k^T)K_{k+1}\frac{\partial \Gamma_k}{\partial T_s}L_k$$

$$- L_k^T\left\{\frac{\partial \Gamma_k}{\partial T_s}K_{k+1}(I-\Gamma_k L_k) + L_k^T\frac{\partial R}{\partial T_s}\right\}L_k$$

(A.2-9)

Substituting Eq. A.2-9 into Eq. A.2-4 one obtains the final result:

$$\frac{\partial K_k}{\partial T_s} = \bar{\theta}_k^T\frac{\partial K_{k+1}}{\partial T_s}\bar{\theta}_k + \bar{\theta}_k^T K_{k+1}\left(\frac{\partial \theta_k}{\partial T_s} - \frac{\partial \Gamma_k}{\partial T_s}L_k\theta_k\right) + \left(\frac{\partial \theta_k}{\partial T_s} - \frac{\partial \Gamma_k}{\partial T_s}L_k\theta_k\right)^T K_{k+1}\bar{\theta}_k$$

$$+ \frac{\partial Q_k^*}{\partial T_s} + \theta^T L_k^T\frac{\partial \hat{R}_k}{\partial T_s}L_k\theta_k$$

(A.2-11)

APPENDIX B
MATRICES FOR THE PROTOTYPE PROBLEM

The matrices which describe the vehicle dynamics, disturbance dynamics, and control design of the example of Section 2.5 are presented here*:

Continuous System Dynamics:

$$F = \begin{bmatrix} -0.3970E\text{-}01 & -0.1000E\ 01 & 0.2094E & 0.2207E\text{-}01 \\ -0.2970E\ 00 & -0.4120E\text{-}01 & 0.5000E\text{-}02 & 0.0 \\ -0.2590E\ 01 & 0.1140E\ 00 & -0.2940E\ 00 & 0.0 \\ 0.0 & 0.0 & 0.1000E\ 01 & 0.0 \end{bmatrix} \qquad \text{(B-1)}$$

Fast Control Effectiveness (Aileron):

$$G_f = \begin{bmatrix} -0.4981E\text{-}03 \\ 0.1184E\text{-}01 \\ 0.2390E\ 01 \\ 0.4369E\text{-}04 \end{bmatrix} \qquad \text{(B-2)}$$

Slow Control Effectiveness (Rudder):

$$G_s = \begin{bmatrix} 0.4125E\text{-}02 \\ -0.1649E\ 00 \\ 0.8405E\ 00 \\ -0.4828E\text{-}04 \end{bmatrix} \qquad \text{(B-3)}$$

*The numerical values presented here are given in standard "E format"; the notation EsNN indicates a factor of 10^{SNN}. For example, 0.1000E-02 is equivalent to 0.001.

Process Noise Covariance:

$$Q_d = \begin{bmatrix} 0.0 & 0.0 & 0.0 & 0.0 \\ 0.0 & 0.0 & 0.0 & 0.0 \\ 0.0 & 0.0 & 0.2500E\ 00 & 0.0 \\ 0.0 & 0.0 & 0.0 & 0.0 \end{bmatrix} \qquad \text{(B-4)}$$

Continuous-Time State Weighting Matrix:

$$Q = \begin{bmatrix} 0.1000E\text{-}01 & 0.0 & 0.0 & 0.0 \\ 0.0 & 0.2500E\text{-}02 & 0.0 & 0.0 \\ 0.0 & 0.0 & 0.2500E\text{-}02 & 0.0 \\ 0.0 & 0.0 & 0.0 & 0.4000E\text{-}01 \end{bmatrix} \qquad \text{(B-5)}$$

Continuous-Time Control Weighting Matrix:

$$R = \begin{bmatrix} 0.2500E\ 00 & 0.0 \\ 0.0 & 0.2500E\ 00 \end{bmatrix} \qquad \text{(B-6)}$$

APPENDIX C
MATRICES FOR THE EXAMPLE SYSTEM

The matrices which describe the vehicle dynamics, disturbance dynamics, and control design of the example of Section 3 are presented here* (Flight Condition: V = 999 ft/sec; h = 20,000 ft).

C.1 AIRCRAFT/DISTURBANCE DESCRIPTION (Eqs. 3.2-2 THROUGH 3.2-5)

Continuous-Time Aircraft/Control Dynamics:

$$\tilde{F} = \begin{bmatrix} 0.0 & 0.0 & 0.1000E\ 01 & 0.0 \\ -0.5615E\ 00 & -0.1069E-01 & -0.8830E-01 & 0.4301E-01 \\ 0.0 & -0.1681E-02 & -0.1141E\ 01 & -0.6618E\ 00 \\ -0.2050E-02 & -0.5946E-01 & 0.1754E\ 02 & -0.1375E\ 01 \end{bmatrix} \qquad (C.1\text{-}1)$$

Disturbance Dynamics:

$$F_d = \begin{bmatrix} -0.5709E\ 00 & 0.5709E\ 00 \\ 0.0 & -0.5709E\ 00 \end{bmatrix} \qquad (C.1\text{-}2)$$

*The numerical values presented here are given in standard "E format"; the notation EsNN indicates a factor of 10^{SNN}. For example, 0.1000E-02 is equivalent to 0.001.

Coupling Dynamics:

$$\tilde{F}_c = \begin{bmatrix} 0.0 & 0.0 \\ 0.4590E\text{-}01 & -0.2891E\text{-}02 \\ -0.6244E\ 00 & -0.3736E\ 01 \\ -0.1949E\ 01 & 0.5744E\ 00 \end{bmatrix} \qquad (C.1\text{-}3)$$

Continuous-Time Control Effectiveness:

$$\tilde{G} = \begin{bmatrix} 0.0 & 0.0 \\ 0.2358E\ 00 & -0.3895E\ 00 \\ -0.1805E\ 02 & -0.1135E\ 02 \\ -0.2554E\ 01 & -0.4691E\ 01 \end{bmatrix} \qquad (C.1\text{-}4)$$

Process Noise Influence:

$$\Lambda_d = \begin{bmatrix} 0.0 \\ 0.3050E\ 01 \\ -0.3739E\text{-}01 \\ -0.3302E\text{-}03 \\ -0.4266E\text{-}02 \\ 0.6560E\text{-}01 \end{bmatrix} \qquad (C.1\text{-}5)$$

C.2 CONTROL DESIGN

Continuous-time Augmented State (vehicle state and control) Weighting Matrix:

$$Q = \begin{bmatrix} 0.1050E\text{-}01 & 0.2315E\text{-}04 & 0.5575E\text{-}04 & 0.2745E\text{-}03 & 0.3699E\text{-}03 & 0.1418E\text{-}02 \\ 0.2315E\text{-}04 & 0.4039E\text{-}01 & -0.6823E\text{-}03 & 0.9083E\text{-}02 & 0.1687E\text{-}01 & 0.3100E\text{-}01 \\ 0.5575E\text{-}04 & -0.6823E\text{-}03 & 0.3703E\text{-}02 & -0.1583E\text{-}01 & -0.2940E\text{-}01 & -0.5389E\text{-}01 \\ 0.2745E\text{-}03 & 0.9083E\text{-}02 & -0.1582E\text{-}01 & 0.2117E\ 00 & 0.3902E\ 00 & 0.7166E\ 00 \\ 0.3699E\text{-}03 & 0.1687E\text{-}01 & -0.2940E\text{-}01 & 0.3902E\ 00 & 0.7649E\ 00 & 0.1331E\ 01 \\ 0.1418E\text{-}02 & 0.3100E\text{-}01 & -0.5389E\text{-}01 & 0.7166E\ 00 & 0.1331E\ 01 & 0.2485E\ 01 \end{bmatrix} \quad \text{(C.2-1)}$$

Continuous-Time Control Rate Weighting Matrix

$$R = \begin{bmatrix} 0.1111E\ 00 & 0.0 \\ 0.0 & 0.2778E\text{-}01 \end{bmatrix} \quad \text{(C.2-2)}$$

REFERENCES

1. Glasson, D.P., "Research in Multirate Estimation and Control," The Analytic Sciences Corporation, Technical Report No. TR-1356-1, December 1980.

2. Whitbeck, R.F., and Hofmann, L.G., "Analysis of Digital Flight Control Systems with Flying Qualities Applications," Air Force Flight Dynamics Laboratory, Report No. AFFDL-TR-78-115, Vol. 2, September, 1978.

3. Konar, A.F., and Lee, J.F., "Analysis of Multiloop, Multirate Digital Control Systems," 1976 IEEE Conference on Decision and Control (Clearwater, FL) December, 1976.

4. Saxe, R., "DIGIKON: The Direct Digital Control System Analysis Program for Shuttle," 1976 IEEE Conference on Decision and Control (Clearwater, FL) December 1976.

5. Franklin, G.F., and Powell, J.D., Digital Control of Dynamic Systems, Addison-Wesley, Reading, MA, 1980.

6. Anon., "Flying Qualities of Piloted Airplanes," Military Specification No. MIL-F-8785B(ASG), 7 August 1969, pp. 47-52.

7. Stengel, R.F., Broussard, J.R., Berry, P.W., and Taylor, J.H., "Modern Methods of Aircraft Stability and Control Analysis," The Analytic Sciences Corporation, Technical Report No. TR-612-2 (Also Office of Naval Research Report No. ONR-CR215-237-2), May 1977.

8. "Background and User's Guide for MIL-F-9490," The Boeing Company, January 1975.

9. Dahlberg, T., "Comparison of Ride Comfort Criteria for Computer Optimization of Vehicles Travelling on Randomly Profiled Roads," Vehicle System Dynamics, Volume 9, No. 6, December, 1980.

10. Levis, A.H. et. al., "On the Behavior of Optimal Linear Sampled-Data Regulators," International Journal of Control, Vol. 13, No. 2, 1971, pp. 343-361.

DISTRIBUTION LIST

Office of Naval Research
800 N. Quincy St.
Arlington, VA 22217
S.L. Brodsky, Code 411 1
C.J. Holland, Code 411 3

Office of Naval Research
Eastern/Central Regional Office
495 Summer St.
Boston, MA 02210 1

Office of Naval Research
Western Regional Office
1030 E. Green St.
Pasadena, CA 91106 1

Naval Research Laboratory
Washington, D.C. 20375
Code 2627 3

Naval Air Systems Command
Washington, D.C. 20361
D. Kirkpatrick, AIR 320D 1
G. Heiche AIR 424 1
R.C. A'Harrah, AIR 904

Naval Air Development Center
Warminster, PA 19874
C.J. Mazza, Code 6053 1
C.R. Abrams, Code 6072 1

Naval Material Command
Washington, D.C. 20360
Code 08T23 1

Naval Weapons Center
China Lake, CA 93555
B. Hardy, Code 3914 1

Naval Surface Weapons Center
Silver Spring, MD 20910
J. Wingate, Code R44 1

David Taylor Naval Ship R&D Center
Bethesda, MD 20084
Technical Library 1

Naval Post Graduate School
Monterey, CA 93940
Technical Reports Library 1
L. Schmidt 1

Defense Technical Information Center
Building 5
Cameron Station
Alexandria, VA 22314 12

Air Force Office of Scientific Research
Building 410
Bolling Air Force Base
Washington, D.C. 20332
G.W. McKemie 1

Air Force Flight Dynamics Laboratory
Wright-Patterson Air Force Base
Dayton, OH 45433
R.E. Ettinger, AFWAL/FIG 1
F. George, Control Dyn. Div. 1
R. Schwanz, AFWAL/FIGC 3

Air Force Institute of Technology
Wright-Patterson Air Force Base
Dayton, OH 45433
P. Maybeck 1

NASA Langley Research Center
Hampton, VA 23665
Technical Library 1
J. Chambers, MS 355 1
J. Elliot, MS 152A 1
J. Newsom 1

Naval Air Test Center
Patuxent River, MD 20670
J. McCue, Code TPS 1

University of Michigan
Dept. of Naval Architecture &
Marine Engr.
Ann Arbor, MI 48109
M.G. Parsons
1

Nielsen Engineering &
Research, Inc.
510 Clyde Avenue
Mountain View, CA 94043
J.N. Nielsen 1

The C.S. Draper Laboratory,
Inc.
555 Technology Square
Cambridge, MA 02139
R.V. Ramnath 1

Michigan State University
Department of Mathematics
106-A Wells Hall
E. Lansing, Michigan 48824
Prof. Bakhtiar Litkouhi 1

NASA Dryden Research Center
P.O. Box 273
Edwards, CA 93523
Technical Library 1
K. Szalai, Code E-EDC 1
K. Peterson, Code E-EDC

National Transportation Safety Board
Bureau of Technology
Laboratory Services Division
800 Independence Ave. SW
Washington, D.C. 20594
R. Von Husen 1

University of Notre Dame
Dept. of Electrical Engineering
Notre Dame, IN 46556
M.K. Sain 1

Flight Research Laboratory
Dept. of Mechanical & Aerospace Eng.
Princeton University
Princeton, NJ 08544
R.F. Stengel 1

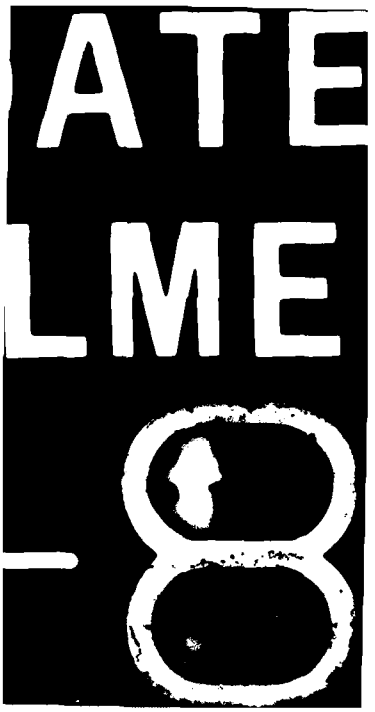
ATE
LME
8